
Volume 18 Issue 4 November 2010 ISSN 1342-937X
ELSEVIER
2009 IF:
4.605
International Geoscience Journal
GONDWANA
RESEARCH
http://elsevier.com/locate/gr
IAGR

Gondwana Research 18 (2010) 596–610

Contents lists available at ScienceDirect

Gondwana Research

journal homepage: www.elsevier.com/locate/gr

Permian basaltic rocks in the Tarim basin, NW China: Implications for plume–lithosphere interaction

Yutao Zhang *, Jiaqi Liu, Zhengfu Guo

Key Laboratory of Cenozoic Geology and Environment, Institute of Geology and Geophysics, Chinese Academy of Sciences, Beijing 100029, China

ARTICLE INFO

Article history:
Received 30 August 2009
Received in revised form 17 March 2010
Accepted 21 March 2010
Available online 30 March 2010

Keywords:
Tarim basin
Oceanic island basalts (OIB)
Large igneous province (LIP)
Mantle plume
Geochemistry

ABSTRACT

There are large areas of Permian basaltic rocks in the Tarim basin (PBRT) in northwestern China. Precise Ar–Ar dating of these rocks revealed an eruption age span of 262 to 285 Ma. Most of the PBRT is composed of alkaline basaltic rocks with high TiO_2 (2.43%–4.59%, weight percent), high Fe_2O_3+FeO (12.63%–17.83%) and P_2O_5 (0.32%–1.38%) contents. Trace elements of these rocks have affinities with oceanic island basalts (OIB), as shown in chondrite normalized rare earth elements (REE) diagrams and primitive mantle normalized incompatible elements diagrams. The rocks show complex Sr–Nd isotopic character based on which they can be subdivided into two distinct groups: group 1 has relatively small initial (t = 280 Ma)^{87}Sr/^{86}Sr ratio (~0.7048) and positive εNd(t) (3.42–4.66) values. Group 2 has relatively large initial ^{87}Sr/^{86}Sr ratio (0.7060–0.7083) and negative εNd(t) (from −2.79 to −2.16) values. Lead isotopes are even more complex with variations of (^{206}Pb/^{204}Pb)t, (^{207}Pb/^{204}Pb)t and (^{208}Pb/^{204}Pb)t ranging from 17.9265 to 18.5778, 15.4789 to 15.6067 and 37.2922 to 38.1437, respectively. Moreover, these two groups have different trace elements ratios such as Nb/La, Ba/Nb, Zr/Nb, Nb/Ta and Zr/Hf, implying different magmatic processes. Based on the geochemistry of basaltic rocks and an evaluation of the tectonics, deformation, and the compositions of crust and lithospheric mantle in Tarim, we conclude that these basaltic rocks resulted from plume–lithosphere interaction. Permian mantle plume caused an upwelling of the Tarim lithosphere leading to melting of the asthenospheric mantle by decompression. The magma ascended rapidly to the base of lower crust, where different degrees of assimilation of OIB-like materials and fractionation occurred. Group 1 rocks formed where the upwelling is most pronounced and the assimilation was negligible. In other places, different degrees of assimilation and fractionation account for the geochemical traits of group 2.

1. Introduction

Basaltic magmatism is one of the fundamental geological processes through time and amongst the various kinds of basalts, alkaline basalt is thought to have originated since the Proterozoic (Condie, 1985, 1989) and has unique geological implications. There are large areas of Permian basaltic rocks in the Tarim basin (PBRT), in northwestern China (Fig. 1). The PBRT are important for understanding the lithospheric evolution of the Tarim Block during the Permian. However, the mechanism of formation of the PBRT is controversial and several hypothesis have been proposed, such as continental rifting (Chen et al., 1997b), within-plate extension (Jiang et al., 2004b; Yang et al., 2007), subduction-related (Yang et al., 2005), and plume-related (Chen et al., 2006; Zhou et al., 2009). These studies however, do not provide adequate information on which the origin and emplacement mechanism of PBRT can be resolved. Moreover, the earlier studies were mostly confined to outcrop samples, and systematic geochronological and geochemical investigations of Permian igneous rocks recovered from borehole are lacking. In this contribution we have integrated data derived from both outcrop and borehole samples. We present new geochronological, geochemical and isotopic data of PBRT and investigate their probable origin. Possible links between Permian igneous activity in the Tarim and other large igneous provinces (LIP), such as the Siberia trap and Emeishan LIP are also discussed.

2. Geological background

Located in the northwestern China, the Tarim Craton is one of the three main cratons in China, the other two being North China Craton and Yangtze Craton. Until now, the position of the Tarim Craton in relation to other important terranes in pre-Paleozoic times was not clear (Huang et al., 2005). Once part of the Rodinia and Pangea supercontinents (Rogers and Santosh, 2003; Santosh et al., 2009), the Tarim has a key role in their reconstruction. Tarim Craton is bound by Tianshan Mountains to the north, Kunlun Mountains to the southwest and Altyn Tagh Mountains to the southeast and is adjacent to the Central Asia Orogenic Belt (CAOB) (Sengör et al., 1993; Xiao et al., 2004, 2010) (Fig. 1). Recently, many studies have addressed the

* Corresponding author.
E-mail address: ytzhang@mail.iggcas.ac.cn (Y. Zhang).

1342-937X/$ – see front matter © 2010 International Association for Gondwana Research. Published by Elsevier B.V. All rights reserved.
doi:10.1016/j.gr.2010.03.006

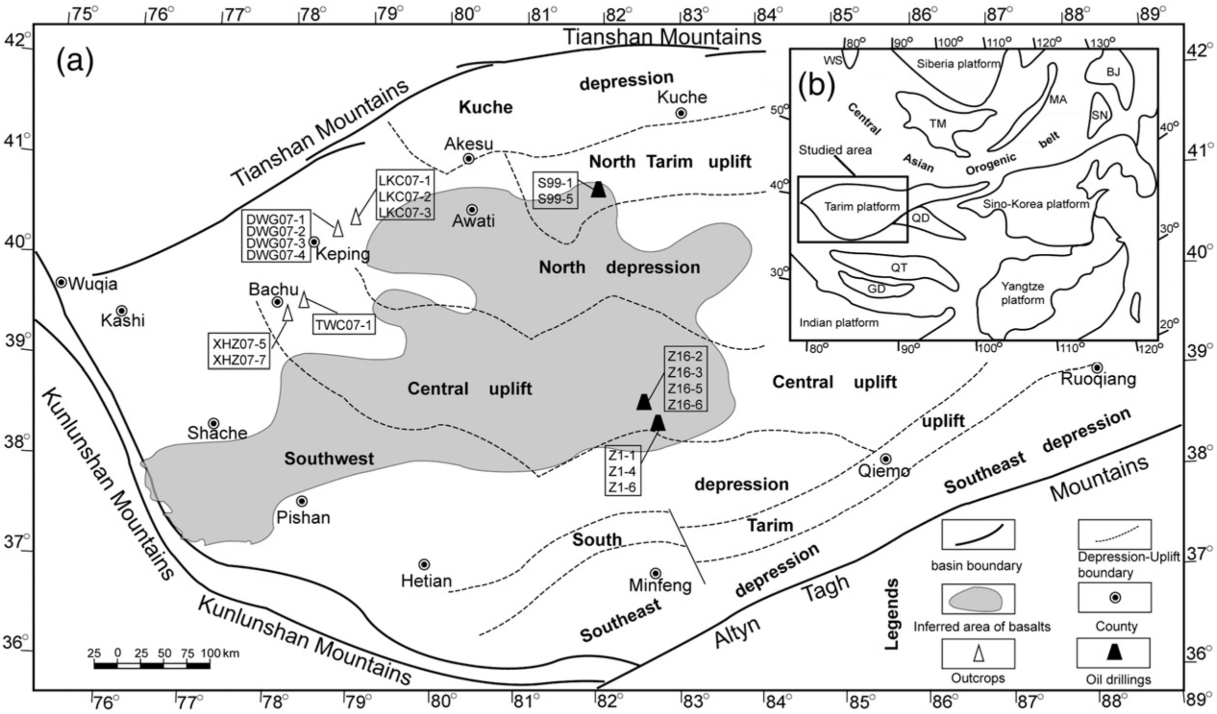

Fig. 1. Sample locations of Permian basaltic rocks in the Tarim basin (a) (after Jia, 1997). Shaded area represents the inferred distribution of basalts in the Tarim basin (from Yang et al., 2005; Chen et al., 2006). Also shown is the position of the Tarim in relation to other tectonic units (b) (after Wang et al., 2006b). Abbreviations for terranes: WS: West Siberian; TM: Tuva-Mongolia, QT: Qiangtang; QD: Qaidam; GD: Gangdise; MA: Central Mongolis-Argun; BJ: Bureya-Jiamusi; SN: Songnen.

geodynamic processes and metallogenesis in central Asia and related orogenic belts (Han et al., 2006; Charvet et al., 2007; Chai et al., 2009; Shen et al., 2009; Zhang et al., 2009b,c; Zhao et al., 2009a,b; Xiao and Kusky, 2009).

In general, the Tarim Block consists of a Precambrian basement (Tarim Craton) and overlying sedimentary rocks. The Precambrian basement rocks formed in Archaean, Palaeoproterozoic, Mesoproterozoic and Neoproterozoic (Lu et al., 2008) and they crop out mainly around Kuluketage, Keping, Tiekelike and Altyn (Jia, 1997). However, Neoproterozoic rocks were reported not only along the margins of the Tarim Craton, but also from Central Tarim (Song et al., 2003; Guo et al., 2005; Li et al., 2005) and West Kunlun (Zhang et al., 2003a,b). According to the investigations, the basement rocks of the Tarim craton could be as old as 3665 Ma (Lu et al., 2008). Overlying the basement are the sedimentary sequences of the Tarim basin, which is a composite and stacked basin (Jia and Wei, 2002). Several uplifted regions and depressions can be recognized, such as the north Tarim uplift, central uplift, and south Tarim uplift; as well as the Kuche depression, north depression, southwest depression and southeast depression (Jia, 1997) (Fig. 1). Faults are well developed in the Tarim basin (Li et al., 2008a) and may have a close relationship with the eruption of PBRT. Based on the strata they intersect, these faults can be subdivided into basement faults and cover faults, which controlled sedimentation and distribution of the volcanic rocks. According to the Xinjiang Bureau of Geology and Resources (1993), Permian basaltic rocks are subdivided into the lower to middle Permian Kupukuziman Formation and the overlying middle Permian Kaipaizileike Formation. PBRT is located mainly in the central and southwestern Tarim (Yang et al., 2005; Chen et al., 2006) (Fig. 1), with outcrops of PBRT mainly expose at Keping and Bachu. As most of these rocks are covered by aeolian deposits, it was difficult to collect samples. This situation changed recently when large scale oil exploration revealed abundant PBRT occur under thick sediments. Permian igneous rocks in the Tarim basin mainly exposed at Keping and Bachu, having been reported by many authors (Yang et al., 1996, 2006, 2007; Chen et al., 1997b, 2006; Jiang et al., 2004a,b,c; Li, 2007; Li et al., 2008b; Zhou et al., 2009). According to previous research, the rock types of this Permian igneous activity are complex, including basalt, diabase, dacite, syenite, etc., although the dominant rocks are alkaline basaltic rocks.

3. Sampling and petrology

With the help of the China Petroleum & Chemical Corporation (SINOPEC), we were able to collect drill core samples in north and central Tarim basin. Drill cores came from one well in north Tarim (S99) and two wells in central Tarim (Z1 and Z16), with outcrop samples coming from Keping and Bachu. Altogether, nineteen specimens were chosen for the study. The location of these samples is shown in Fig. 1. All the samples are fresh, except for LKC07-3, which contains small amygdales.

Samples from Keping (LKC and DWG series) belong to the Kupukuziman formation, which is underlain by sedimentary rocks of unknown age (probably Carboniferous). At Linkuangchang (LKC) district, only basalts were found, in contrast to discoveries at Dawangou (DWG), where both basalts and diabases occur. The diabase dike in Dawangou intrudes Silurian carbonates. The contacts are sharp with evidence of extensional environment and fast emplacement. Diabase samples were also collected from Tangwangcheng (TWC) and Xiaohaizi (XHZ) in Bachu. The Tangwangcheng diabase is similar to that collected from Dawangou, but has a more intimate relationship with peripheral carbonates. Hundreds of diabase dikes were emplaced in the Xiaohaizi sedimentary carbonates and these dikes are all fine-grained compared to those in Dawangou and Tangwangcheng. In fact, the texture of the Xiaohaizi diabase is very fine and for this reason the diabase can be considered as a subvolcanic rock.

Samples from wells S99, Z1 and Z16 are all basaltic rocks. In the original log record of wells S99, Z1 and Z16, S99-1 belong to the Carboniferous, Z1-6 belongs to the Silurian, Z16-2, Z16-3, Z16-5 and Z16-6 belong to the Ordovician. S99-1, Z1-6, Z16-2, Z16-3, Z16-5 and Z16-6 are all fine-grained diabase. Age determinations show that they are all Permian. The other three (S99-5, Z1-1 and Z1-4) well basalts were assigned a Permian age in the log record.

All samples were thin sectioned and examined under a polarizing microscope. The basalts (and fine-grained diabases) are fine-grained and have a porphyritic texture with phenocrysts of plagioclase, clinopyroxene and olivine. The groundmass consists of fine-grained to aphanitic minerals and opaque oxides. Typical diabases are DWG07-1 and TWC07-1 with grain sizes larger than those of the basalts and having more euhedral mineral phases. Photomicrographs of representative basalt (LKC07-1) and diabase (TWC07-1) are shown in Fig. 2.

4. Analytical methods

4.1. $^{40}Ar/^{39}Ar$ dating

Groundmasses of seven igneous rocks were dated by the step-heating $^{40}Ar/^{39}Ar$ method. Fresh rock samples were crushed so that they passed through 60–80 mesh. Phenocrysts were eliminated using a binocular microscope. Groundmass material was further purified by ultrasonic cleaning machine. The solvents were water and acetone successively. Interestingly, several samples appeared cloudy even after more than 10 purification cycles. Considering that there are huge amounts of carbonates in the Tarim basin, the difficulties encountered in cleaning samples may be attributed to the entry of micro carbonate specks. Later we realized that the age results are not satisfactory which can be seen in age plateau and inverse isochron diagrams. Groundmass grains weighing 3–16 mg were sent to the Beijing Atomic Energy Research Institute for irradiation. The J value for these samples is 0.0061500 ± 0.0000154. Bern4M was used as age standard, which yielded an age of 18.700 ± 0.056 Ma.

After irradiation, these powders were dated at the Institute of Geology and Geophysics, Chinese Academy of Sciences (IGGCAS), Beijing. Specks from the powders were placed into a Ta tube resting in the Ta crucible of an automated double-vacuum resistance furnace. These were incrementally heated in 15 steps of 10 min each from 700 or 750 °C to 1400 or 1500 °C. Following 5 additional minutes of gas purification on Al–Zr getters, isotopic measurements were made on a mass spectrometer MM5400. Plateau ages were determined from 3 or more contiguous steps, comprising >50% of the ^{39}Ar released, revealing concordant ages at the 95% confidence level. The uncertainties in plateau ages reflect multiplication by the MSWD and were obtained by standard weighting of errors for individual steps according to their variance (Taylor, 1982). Inverse isochron ages were calculated from the plateau steps using the York (1969) regression algorithm. More details of $^{40}Ar/^{39}Ar$ dating method can be found in Wang et al. (2006a).

4.2. Geochemical analysis

All samples were crushed so that they passed through 200mesh by an agate disintegrator at the Institute of Regional Geology and Resource Survey, Langfang, Hebei Province, China. Geochemical analysis, including major elements, trace elements and Sr–Nd–Pb isotopes were all performed at the Institute of Geology and Geophysics, Chinese Academy of Sciences.

Major element analysis was carried out by XRF using fused glass discs. The precision and accuracy of the major-element data of the Chinese whole-rock basalt standard GSR-3 (Xie et al., 1989) are ≤3% and ca. 5% (2σ), respectively. The FeO concentration was determined using conventional titration procedure.

Trace elements were measured by inductively coupled plasma mass spectrometry (ICPMS) with a Finnigan MAT Element II mass spectrometer. Samples were digested with a mixture of HF and HNO_3 acids in screw-top PTFE-lined stainless steel bombs at 185 °C for two days, and insoluble residues were dissolved in HNO_3 acid heated to 145 °C for 3 h. The closed high-pressure bombs were used to ensure complete digestion. Precision for all trace elements is estimated to be 5% and accuracy is better than 5% for most elements established through analyses of the GSR-3 standard.

About 100–150 mg whole rock powder was completely decomposed in a mixture of HF–$HClO_4$ for Sr–Nd isotopic analysis, and in a mixture of HF–HNO_3 for Pb isotopic analysis. Dissolution was done at 200° for 7 days. Chemical separation and isotopic measurements were carried out following the procedures outlined in Hegner et al. (1995). Sr and LREE were separated in quartz columns with a 5 ml resin bed of AG 50 W-X12, 200–400 mesh. Nd was separated from Sm in quartz columns using 1.7 ml Teflon® powder coated with HDEHP® as the cation exchange medium. Pb was separated in Teflon® columns containing 80 µl AG1-X8, 100–200 mesh and employing a HBr–HCl wash and elution procedure. Procedural blanks were <200 pg for Sr, <50 pg for Pb, and ~30 pg for Nd. Sr–Nd–Pb isotopic data were measured using a MAT 262 mass spectrometer. The Sr and Nd isotope ratios were normalized to $^{86}Sr/^{88}Sr = 0.1194$ and $^{146}Nd/^{144}Nd = 0.7219$. The La Jolla standard yielded $^{143}Nd/^{144}Nd = 0.511862 \pm 10$ (2 sigma, $n = 13$) and NBS-987 gave $^{87}Sr/^{86}Sr = 0.710240 \pm 11$ (2 sigma, $n = 6$). The $^{87}Rb/^{86}Sr$ and $^{147}Sm/^{144}Nd$ ratios were calculated using the Rb, Sr, Sm and Nd abundances. Measured Pb isotopic ratios were corrected for instrumental mass fractionation of 0.1% per atomic mass unit by references to repeated analyses of the NBS-981 Pb standard. Repeated analyses of NBS-981 gave $^{204}Pb/^{206}Pb = 0.05897 \pm 15$, $^{207}Pb/^{206}Pb = 0.91445 \pm 80$, $^{208}Pb/^{206}Pb = 2.16170 \pm 180$ (2 sigma).

5. Analytical results

5.1. Geochronology

Seven specimens have been dated by Ar–Ar method and the results are listed in the Supplementary table. Diagrams of incremental heating plateau age and inverse isochron ages are shown in Fig. 3, from which it is clear that plateau age and inverse isochron age are approximate,

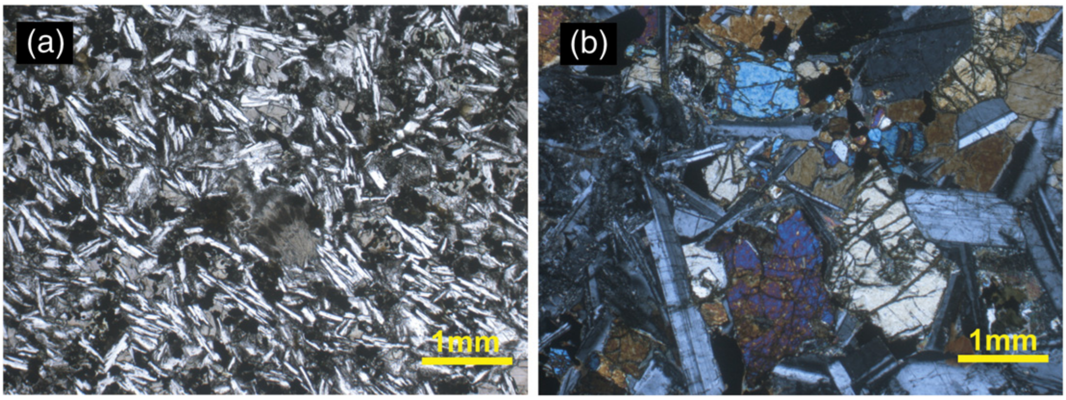

Fig. 2. Typical basalt (LKC07-1) (a) and diabase (TWC07-1) (b) in the Tarim basin. Scale bar has a length of 1 mm.

within errors. The errors of the plateau ages are smaller compared to those of inverse isochron ages, so plateau ages are used in the following discussion. These seven samples all belong to the early Permian except for Z1-6 (269 Ma) and TWC07-1 (262 Ma), which are mid-Permian. Of the five early Permian samples, LKC07-1 and XHZ07-7 are older, with ages exceeding 280 Ma (283 Ma and 285 Ma respectively). The other three early Permian samples have ages ranging from 271 Ma–274 Ma (Z16-2:271 Ma; DWG07-4:272 Ma; DWG07-1:274 Ma). Although the age span of these basaltic rocks seems large (about 23 Ma), it is within the age distribution obtained in other works (Chen et al., 1997a, b, 1998; Jia, 1997; Yang et al., 2006, 2007; Li, 2007).

5.2. Alteration effects on samples

The studied 19 samples and especially the nine specimens collected from drill cores probably underwent some alteration of mafic

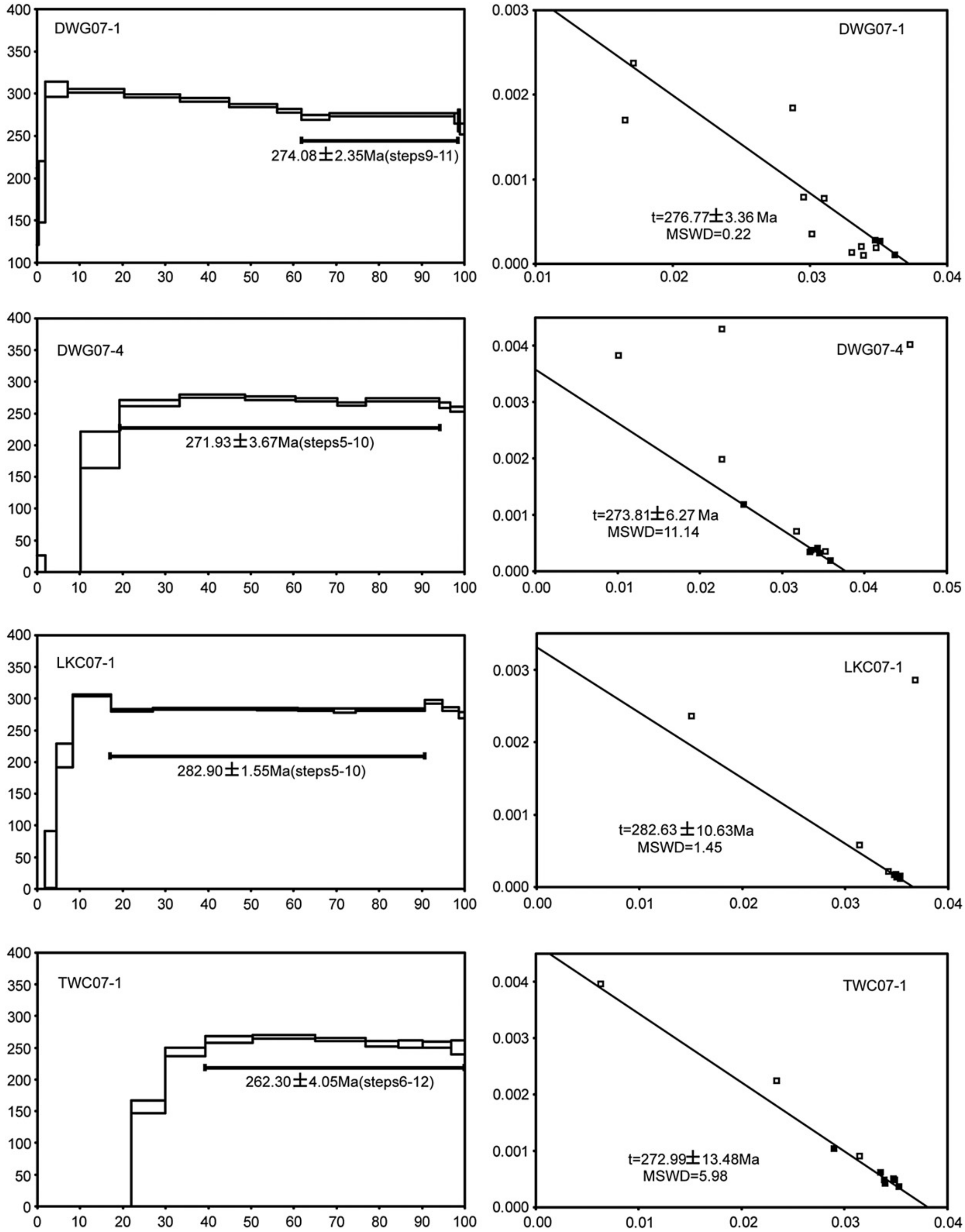

Fig. 3. $^{40}Ar/^{39}Ar$ plateau age (left) and inverse isochron age (right).

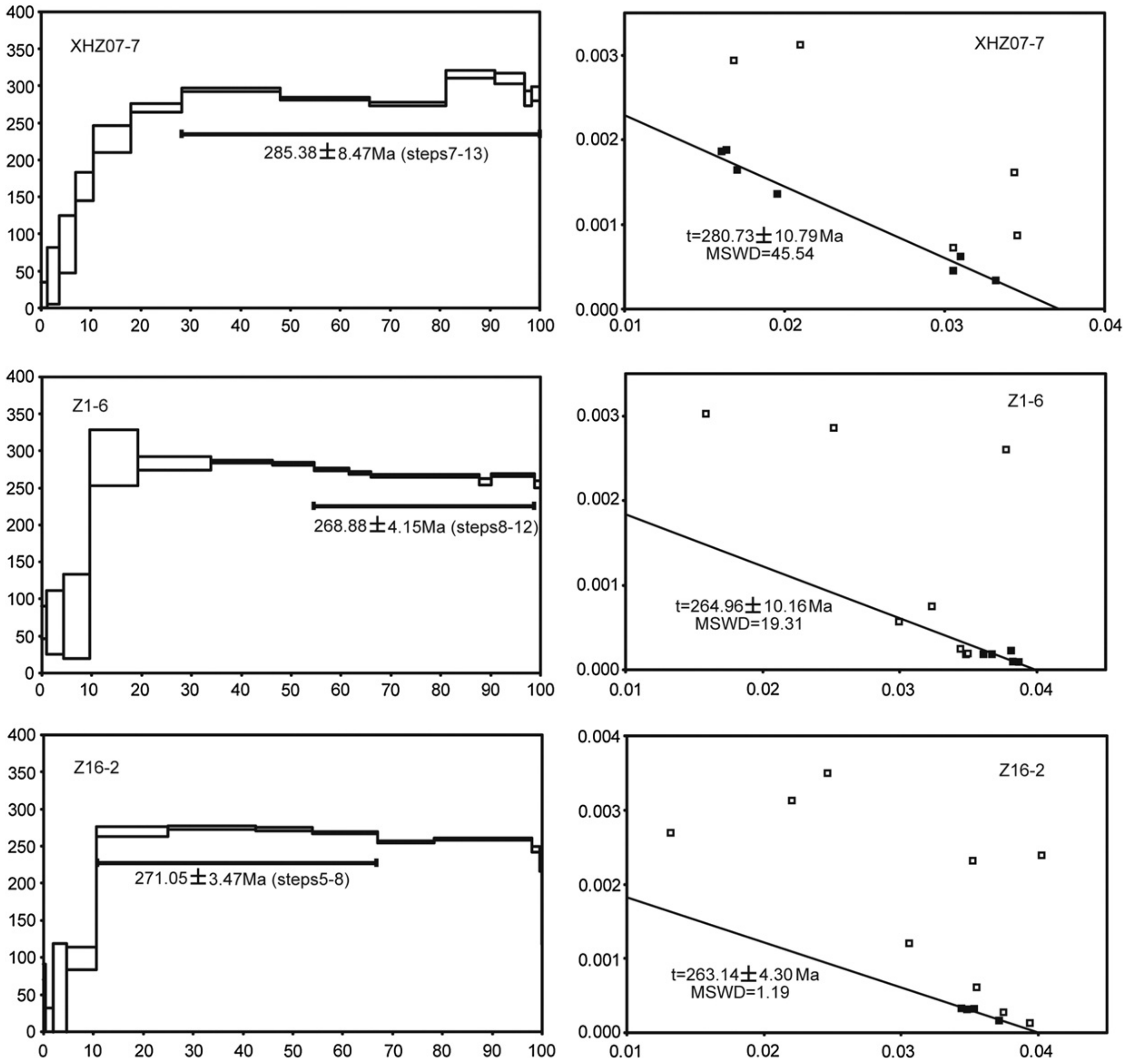

Fig. 3 (*continued*).

minerals, such as pyroxene and olivine. Therefore, before proceeding further it is necessary to test element mobility in these rocks. Elements that are readily mobilized include Ca, Mg, Na, K, Rb, Ba, Pb and U, whereas Zr, Hf, Nb, Ta, Y, Yb, Ti, Cr, P, Ni, Rare Earth Elements (REE) and Th are considered to be relatively immobile (Winchester and Floyd, 1977; Floyd and Winchester, 1978; Pearce, 1982, 1996; Polat et al., 2002). Amongst relatively immobile elements Zr is generally considered to be the most immobile in mafic igneous rock during low-to medium-grade seafloor-hydrothermal alteration (Wood et al., 1979; Gibson et al., 1982). In order to assess elemental mobility, selected trace elements and major element oxides were plotted against Zr (Fig. 4). If an element shows a good correlation with Zr on such variation diagrams it is considered immobile. In Fig. 4, good correlations exist between Zr and Nb, Y, Hf, Sm, Ce, La, Ta, Yb and TiO_2. Whereas for K_2O, Na_2O, Ba, Th, U and Pb, there seems no linear correlation with Zr. Thus, in the following discussion only these relatively immobile elements are used.

5.3. Major elements and rock classification

Major element analysis results are listed in Table 1. The SiO_2 contents of these rocks range from 40.67% to 50.67% (wt.%). Special attention should be paid to LKC07-3 because it has the highest SiO_2 contents, which may be ascribed to the silica filled amygdules. These rocks have a high TiO_2 content (2.43%–4.59%) comparable to that of high Ti basalts in Emeishan large igneous province (LIP) (Xu et al., 2001) but differ drastically from those of island arc volcanic rocks. The contents of TFe (sum of Fe_2O_3 and FeO) are high (12.63%–17.83%). The MgO contents are low (3.25%–6.01%) and the Mg# value (Mg/(Mg + Fe^{2+}), atomic ratio, recalculated to 100% anhydrous) of these rocks have a variation of 0.37–0.60, which means that the magma cannot be primary. The total alkali contents show a range of 6.86% to 3.46%, with most being about ~4%. Na_2O contents are much higher than K_2O contents, with Na_2O/K_2O values of 1.34 to 11.10. Another striking aspect of these samples is their high P_2O_5 contents (up to 1.32%), which means apatite is not a main fractionated mineral. They are similar to the high Ti–P type in the Emeishan LIP (Zhang and Wang, 2002). Loss on ignition (LOI) of these samples has a large variation, from 0.46% (DWG07-2) to 6.02% (Z16-6). Nine samples were collected from drill cores and they probably underwent severe hydrothermal alteration, therefore their LOI (>2%) are higher than outcrop samples as can be seen in Table 1.

Because of the high LOI contents and the mobility of K_2O and Na_2O of these rocks as displayed in Fig. 4, we prefer not use the TAS diagram and instead the $Zr/(TiO_2 \times 10{,}000) - Nb/Y$ (Winchester and Floyd, 1977) diagram was chosen for rock classification. In Fig. 5, 17 samples

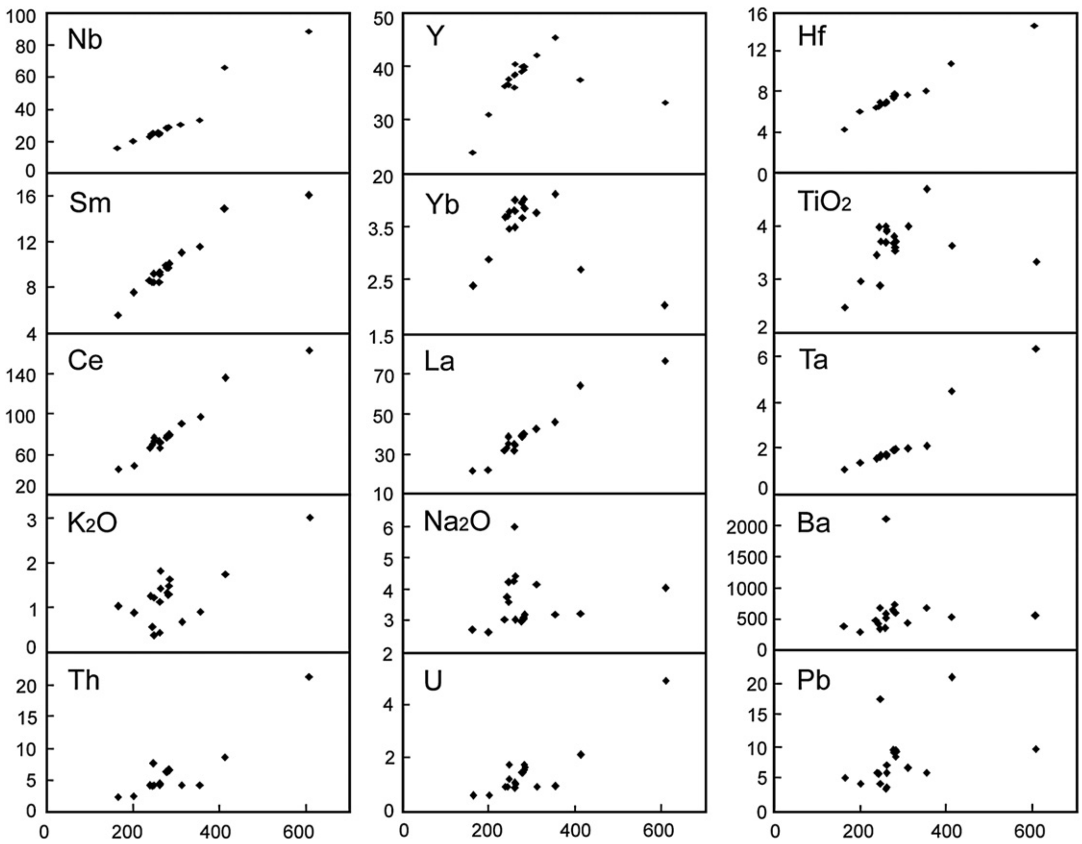

Fig. 4. Plots of some elements/oxides vs. Zr to evaluate the mobility of these elements/oxides of different geochemical behavior during alteration.

cluster near the border between subalkaline and alkaline areas, with two exceptions (XHZ07-5 and XHZ07-7). Of the 17 samples, most are alkaline basalts and fall into the reference range (Chen et al., 1997b; Jiang et al., 2004a,b,c; Li et al., 2008b; Zhou et al., 2009) of PBRT. Samples XHZ07-5 and XHZ07-7 seem to be more alkaline because they plot far from the other 17 samples, with XHZ07-5 plotting into the trachyandesite field. Altogether, the main body of PBRT is alkaline, which is consistent with former studies (Chen et al., 1997b; Jiang et al., 2004b,c; Li et al., 2008b; Zhou et al., 2009). Alkaline trait of these samples can also be found in mineral compositions. For example, according to EPMA data, pyroxenes and plagioclases in TWC07-1 are Ti-rich clinopyroxene and sodium-rich plagioclase (unpublished data), which is a character of alkaline basalt.

In the Harker diagram (Fig. 6), negative correlations exist between SiO_2 and TiO_2, TFe (Fe_2O_3+FeO), CaO, P_2O_5, Al_2O_3 and MgO, which imply that pyroxene, olivine and apatite may have fractionated before the emplacement of these rocks. However, relationships between SiO_2 and K_2O, Na_2O are ambiguous, although there are weak positive correlations.

5.4. Trace elements

The results of trace element analysis are listed in Table 1. Distinct trace elements characteristics of these rocks include: low contents of transitional metallic elements such as Cr (6.8 ppm–118.9 ppm) and Ni (33.7 ppm–65.1 ppm), large variation of total rare earth elements (REE) contents (124 ppm–393 ppm) and trace elements ratios such as Nb/La (0.63–1.16), Ba/Nb (6.35–83.68) and Zr/Nb (6.27–10.86). According to the REE, high field strength elements (HFSE) and incompatible element compositions, three rock types can be identified. Type 1 includes DWG07-4 and TWC07-1, having the lowest contents of REE (from La to Er) and incompatible elements such as Nb, Ta, Zr, Hf, Y, Th and U etc. Type 2 includes XHZ07-5 and XHZ07-7 which are characterized by highest REE (from La to Dy) contents and incompatible elements such as Rb, Th, U, Nb, Ta, Zr and Hf etc. The remaining fifteen samples are of type 3, with REE and some incompatible elements compositions between types 1 and 2. Though contents of most REE and incompatible elements of type 3 lie between those of type 1 and type 2, the heavy REE contents such as Ho, Er, Tm, Yb, Lu of S99-5 are the highest among all the samples. The reason for this seemingly abnormal phenomenon may be ascribed to eclogitic micro xenoliths, such as that found in dacite from well T453 (unpublished data).

Chondrite normalized REE patterns (Fig. 7a for outcrops and Fig. 7b for drill cores) of all samples are LREE enriched with type 2 (XHZ07-5 and XHZ07-7) having the largest fractionation between La and Yb [$(La/Yb)_N=25.6$ and 16.0 respectively)]. Eu anomalies are slight for all the samples ($\delta Eu=0.88$–1.02). It is clear from Fig. 7a that REE contents of type 2 are higher than those of type 1 and type 3 with type 1 lying at the bottom. REE patterns of N-MORB, E-MORB and OIB (Sun and Mcdonough, 1989) are also illustrated in Fig. 7. As revealed by Fig. 7, REE patterns of most samples are above those of N-MORB and E-MORB and strongly resemble that of OIB.

Incompatible trace elements are very complex as can be seen in primitive mantle normalized incompatible elements diagrams (Fig. 8a, b). Also plotted are those of N-MORB, E-MORB and OIB (Sun and Mcdonough, 1989). In Fig. 8a, type 3 lies between type 1 and type 2, with type 2 at the top. Samples in Fig. 8a are outcrops and the most conspicuous traits include: Th and U hump of type 2 (especially of XHZ07-5); slightly Nb–Ta depletion of type 1 and type 3 with type 2 having a positive Nb–Ta anomaly and negative Sr and Zr–Hf anomalies. Fig. 8b shows drill core samples, which has positive anomalies of Ba and P, with K and Sr negative anomalies (with Z1-4 has positive K and Z1-1 and Z1-4 have positive Sr anomalies). If these samples are classified as group 1 and group 2 as in the following paragraph, it is clear that the abundance of most trace elements of

Table 1
Major (wt.%) and trace (ppm) elements results of Permian basaltic rocks in the Tarim basin.

Sample	DWG07-1	DWG07-2	DWG07-3	DWG07-4	LKC07-1	LKC07-2	LKC07-3	S99-1	S99-5	TWC07-1	XHZ07-5	XHZ07-7	Z1-1	Z1-4	Z1-6	Z16-2	Z16-3	Z16-5	Z16-6
SiO2	47.97	48.39	47.81	47.85	46.55	47.52	50.67	41.92	42.01	44.58	46.29	48.05	47.57	47.24	44.94	43.22	41.79	42.54	40.67
TiO2	3.69	3.51	3.65	2.93	3.52	3.79	2.79	3.81	4.59	2.43	3.25	3.52	3.56	3.83	3.36	3.78	3.80	3.83	3.47
Al2O3	13.21	13.22	13.21	13.66	12.98	13.39	13.05	13.82	15.39	15.54	12.62	14.16	13.67	13.97	13.97	13.56	13.24	13.53	12.69
Fe2O3	5.95	5.12	5.94	5.87	5.74	5.24	6.80	9.87	10.54	4.29	6.07	5.71	8.36	7.57	6.38	7.48	9.32	8.52	9.13
FeO	10.82	11.59	11.29	10.33	11.63	12.05	7.35	7.40	7.29	10.49	7.94	6.92	5.13	5.80	8.44	8.64	7.70	7.43	6.47
MnO	0.25	0.25	0.26	0.20	0.26	0.27	0.21	0.20	0.30	0.20	0.15	0.21	0.22	0.25	0.21	0.22	0.24	0.22	0.23
MgO	4.12	4.13	4.14	5.61	3.82	4.18	3.25	5.72	3.25	8.64	6.01	4.11	3.49	4.96	5.44	5.39	5.87	5.18	4.67
CaO	7.99	7.97	7.65	8.57	8.28	8.07	7.64	6.82	9.02	7.95	7.59	8.72	6.85	6.86	9.62	9.17	8.77	9.15	10.96
Na2O	3.16	3.02	2.93	2.59	3.04	3.06	3.48	3.95	3.12	2.65	3.93	3.12	5.76	4.29	2.95	2.91	3.57	4.07	3.93
K2O	1.62	1.29	1.31	0.87	1.45	1.28	1.19	0.64	0.89	1.01	2.93	1.68	1.09	1.77	1.21	1.37	0.54	0.42	0.35
P2O5	0.70	0.68	0.71	0.32	0.70	0.71	0.57	1.25	1.38	0.50	0.78	0.76	0.78	0.81	0.68	0.81	0.76	0.77	0.81
LOI	0.50	0.46	0.62	0.92	1.42	0.66	2.42	4.57	2.16	1.14	1.84	2.56	2.92	2.76	2.28	2.90	4.48	3.68	6.02
TOTAL	99.99	99.64	99.50	99.73	99.39	100.22	99.42	99.99	99.96	99.41	99.40	99.51	99.40	100.12	99.47	99.45	100.08	99.33	99.40
Mg#	0.40	0.39	0.40	0.49	0.37	0.38	0.44	0.58	0.44	0.59	0.57	0.51	0.55	0.60	0.53	0.53	0.58	0.55	0.56
V	265.8	263.1	262.9	280.0	256.3	261.9	211.5	196.6	221.6	134.6	191.5	220.5	234.5	226.5	206.6	191.4	182.2	185.0	177.4
Cr	16.31	16.95	14.99	88.75	14.17	14.31	8.53	30.62	32.38	44.19	118.9	6.83	55.99	58.31	88.43	42.32	38.58	40.18	34.52
Co	46.19	45.82	46.29	57.15	47.14	46.64	36.60	46.79	52.70	65.09	33.69	42.50	38.37	39.41	47.57	42.59	40.11	42.84	40.67
Ni	22.88	22.64	22.00	136.25	21.60	22.54	13.11	61.52	64.32	157.2	125.5	25.32	53.55	55.94	78.66	47.66	42.89	45.42	44.69
Cu	32.08	33.11	33.44	213.57	34.91	36.99	20.68	41.42	44.89	25.27	21.23	59.02	24.07	37.40	41.73	35.99	13.82	14.37	15.88
Zn	180.0	176.7	179.5	151.3	181.9	177.4	164.5	161.1	223.5	138.3	132.2	233.2	122.1	179.2	144.8	186.8	146.3	146.8	176.6
Ga	24.11	23.70	23.29	23.74	23.45	24.02	22.09	22.17	25.44	19.32	31.01	28.35	22.49	24.51	22.45	22.75	22.52	22.91	22.28
Rb	31.81	17.94	16.59	18.77	22.88	20.65	20.75	7.59	8.35	18.51	95.19	59.03	23.91	45.41	26.44	34.05	6.80	5.08	5.42
Sr	358.5	591.0	471.8	354.0	317.3	353.4	498.7	231.5	410.8	376.9	981.0	736.3	1061	1182	400.2	359.4	399.6	405.5	412.8
Y	39.94	39.33	38.96	30.85	40.00	39.89	36.42	42.10	45.32	23.71	33.17	37.44	36.01	40.36	36.23	38.50	36.58	38.24	37.48
Zr	283.6	281.9	277.2	201.2	282.0	279.3	247.3	311.9	354.8	164.5	608.2	413.0	261.1	262.2	238.4	261.9	243.8	259.6	247.6
Nb	28.45	28.19	28.07	19.75	28.58	27.74	24.35	30.18	33.16	15.69	88.50	65.86	24.04	25.17	22.59	24.85	24.23	25.28	24.89
Cs	0.26	3.80	2.71	0.67	2.70	3.28	3.50	4.86	0.48	0.49	3.99	3.49	0.63	0.56	0.71	1.33	0.30	0.30	0.37
Ba	611.4	742.4	663.7	300.4	622.0	629.9	685.2	451.6	691.1	397.9	561.6	542.6	589.9	2106	492.6	519.8	427.6	361.3	350.0
La	39.86	40.08	38.98	22.34	39.96	38.93	38.62	42.45	45.76	21.93	76.47	64.01	31.85	34.98	31.98	34.64	33.35	35.37	35.48
Ce	79.54	79.19	76.99	48.81	79.94	78.70	76.74	90.29	97.16	45.57	163.5	135.8	66.64	72.74	66.49	71.88	69.37	72.79	73.02
Pr	11.14	10.97	10.99	7.15	10.85	10.65	10.09	12.23	12.98	6.19	19.93	17.72	9.57	10.49	9.18	10.05	9.40	10.23	9.86
Nd	45.62	45.61	44.89	30.47	44.47	43.65	42.05	51.07	54.58	25.35	81.54	70.25	39.95	43.36	37.86	41.48	38.61	42.98	42.55
Sm	10.05	10.02	9.90	7.52	9.70	9.70	8.45	11.00	11.55	5.55	16.05	14.86	8.47	9.35	8.57	9.14	8.44	9.21	9.15
Eu	2.92	2.92	2.91	2.29	2.94	2.94	2.44	3.17	3.50	1.81	4.77	4.40	2.42	2.68	2.50	2.64	2.46	2.56	2.62
Gd	9.22	9.20	9.03	7.21	9.23	9.06	8.25	9.51	10.40	5.16	13.22	12.86	7.76	8.86	7.54	8.06	7.61	7.99	7.86
Tb	1.39	1.39	1.39	1.14	1.47	1.37	1.23	1.49	1.64	0.79	1.75	1.86	1.20	1.37	1.22	1.30	1.22	1.30	1.32
Dy	8.07	8.18	8.03	6.80	8.44	8.14	7.47	8.87	9.26	4.75	8.44	9.65	7.13	8.21	7.48	7.75	7.41	7.74	7.61
Ho	1.60	1.60	1.60	1.30	1.71	1.58	1.47	1.70	1.86	0.92	1.42	1.64	1.47	1.66	1.53	1.61	1.51	1.60	1.56
Er	4.30	4.30	4.25	3.40	4.39	4.21	3.82	4.38	4.79	2.54	3.07	3.77	3.86	4.35	4.06	4.26	4.08	4.21	4.16
Tm	0.61	0.61	0.61	0.46	0.64	0.60	0.55	0.62	0.66	0.37	0.37	0.47	0.56	0.65	0.59	0.61	0.58	0.61	0.60
Yb	3.84	3.85	3.95	2.88	4.01	3.66	3.45	3.75	4.10	2.38	2.01	2.69	3.48	3.99	3.67	3.79	3.69	3.81	3.76
Lu	0.57	0.58	0.57	0.41	0.59	0.56	0.52	0.57	0.62	0.37	0.27	0.37	0.52	0.61	0.55	0.58	0.56	0.58	0.58
Hf	7.64	7.54	7.53	6.01	7.76	7.32	6.90	7.63	8.04	4.25	14.55	10.76	6.81	6.98	6.41	6.85	6.48	6.79	6.58
Ta	1.94	1.93	1.92	1.36	1.96	1.91	1.61	1.98	2.10	1.07	6.34	4.48	1.66	1.73	1.54	1.70	1.64	1.73	1.68
Pb	9.25	8.46	9.44	4.20	9.55	9.10	17.52	6.68	5.96	5.15	9.63	20.85	5.89	7.15	5.91	3.65	5.75	3.41	4.24
Th	6.55	6.77	6.26	2.47	6.52	6.30	7.62	4.26	4.21	2.36	21.19	8.60	4.19	4.40	4.17	4.31	4.05	4.32	4.23
U	1.65	1.75	1.44	0.60	1.54	1.44	1.75	0.91	0.94	0.59	4.90	2.11	0.87	1.05	0.93	1.00	0.93	1.06	1.21

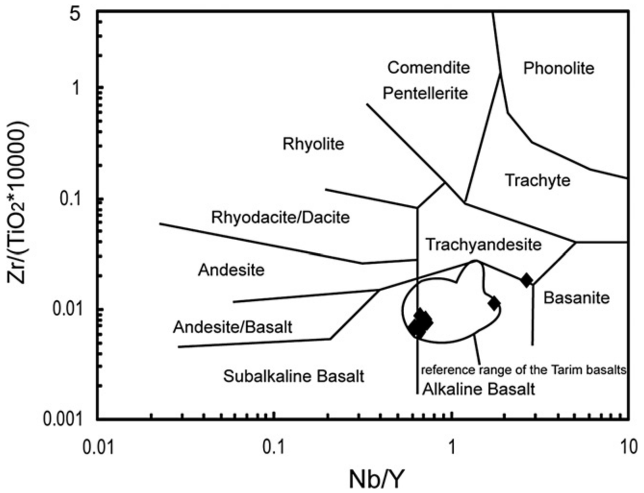

Fig. 5. Classification of Permian basaltic rocks in Zr/($TiO_2 \times 10,000$) − Nb/Y (Winchester and Floyd, 1977) plot (reference data came from Chen et al., 1997a,b; Jiang et al., 2004a, b,c; Li et al., 2008b).

group 2 lies between those of group 1. Because K, Ba and Sr are mobile during hydrothermal alteration, the anomalies of these elements may be ascribed to alteration. For example, Zhu et al. (2008) reported that there is extensive deep fluid activity in the Tarim basin.

5.5. Sr–Nd–Pb isotopes

Ten samples were analysed for Sr–Nd–Pb isotopes and the results are listed in Tables 2 and 3. The initial (t = 280 Ma) $^{87}Sr/^{86}Sr$ values range from 0.7048 (DWG07-4) to 0.7083 (Z1-1) and $\varepsilon Nd(t)$ values from −2.79 (Z16-2) to 4.66 (XHZ07-7). These samples can be further divided into two groups: Group 1 (DWG07-4, XHZ07-5 and XHZ07-7) with relatively small initial $^{87}Sr/^{86}Sr$ ratio (~0.7048) and positive $\varepsilon Nd(t)$ (3.42–4.66), and group 2 for the other 16 samples which have relatively large initial $^{87}Sr/^{86}Sr$ ratio (0.7060–0.7083) and negative $\varepsilon Nd(t)$ (−2.79 to −2.16) values. It should be noted that these two

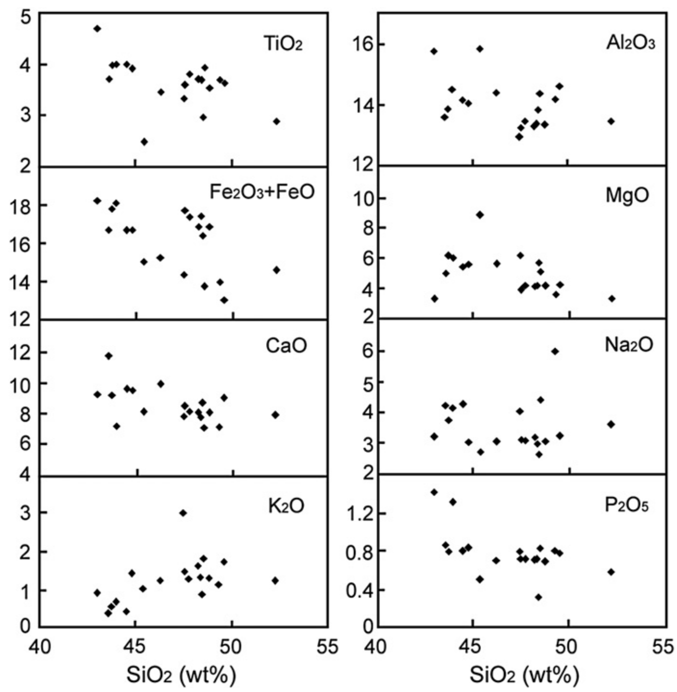

Fig. 6. Harker diagram of Permian basaltic rocks in the Tarim basin.

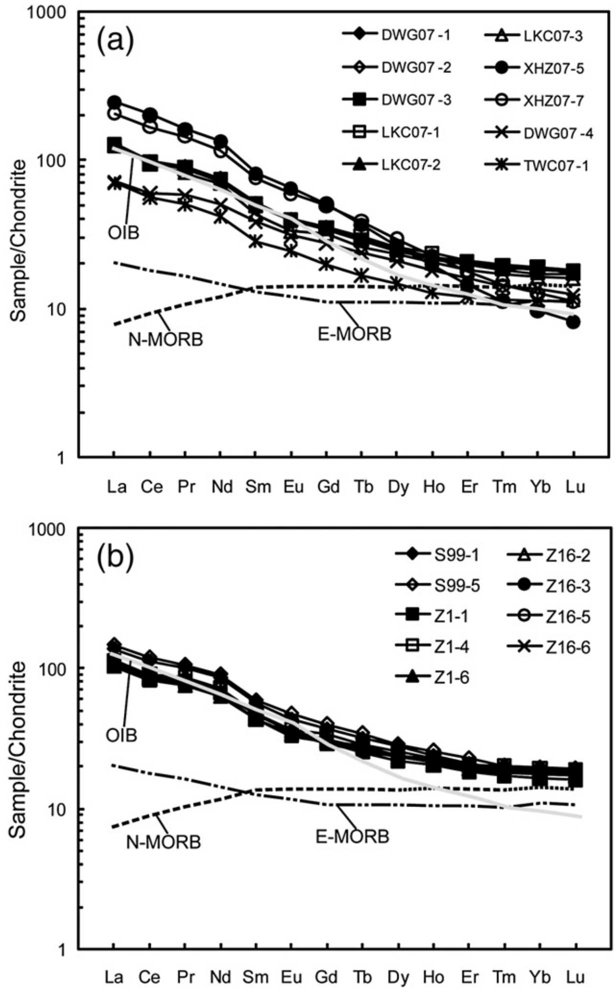

Fig. 7. Chondrite normalized rare earth element patterns of Permian basaltic rocks in the Tarim basin ((a): outcrops, (b): drill well cores). Values of chondrite are from Boynton (1984). Also plotted are patterns of OIB, N-MORB and E-MORB which come from Sun and Mcdonough (1989).

groups were defined for the convenience of discussion as there seems to be no specific spatial or temporal relationship between them. DWG07-4 and TWC07-1 are typical diabases from their major elements results, TWC07-1 is more primitive (e.g., higher MgO contents), but the isotopic data show that DWG07-4 may be more primitive than TWC07-1. Furthermore, ages of DWG07-4 (272 Ma) and TWC07-1 (262 Ma) are quite different, so the paradox in major and isotopic results may reflect either source differences or different degree of contamination by lithospheric materials. DWG07-4 has the lowest initial $^{87}Sr/^{86}Sr$ value but its $\varepsilon Nd(t)$ value is not as large as that of XHZ07-7. Considering that XHZ07-7 is highly enriched in REE and other incompatible elements, this may mean that its source may be depleted mantle metasomatised by relatively young enrichment events. TDM ages change from 704 Ma to 1438 Ma with the former belonging to XHZ07-7 and the latter to Z16-2. Interestingly, most TDM ages fall in the span of 1349 Ma–1438 Ma, except those of DWG07-4 and XHZ07-7 which are 1022 Ma and 704 Ma respectively. This may reflect the heterogeneity of the basement of the Tarim basin.

Lead isotopes are more complex because U, Th and Pb are all mobile during alteration, as illustrated in Fig. 4. Ratios of lead isotopes are low, with variations of $(^{206}Pb/^{204}Pb)t$, $(^{207}Pb/^{204}Pb)t$ and $(^{208}Pb/^{204}Pb)t$ of 17.9265–18.5778, 15.4789–15.6067 and 37.2922–38.1437 respectively, which are smaller than those of the Emeishan picritic and associated basalt flows (Zhang et al., 2006). Group 1 and group 2 cannot be easily distinguished by lead isotopes. Like Sr and Nd isotopes in which

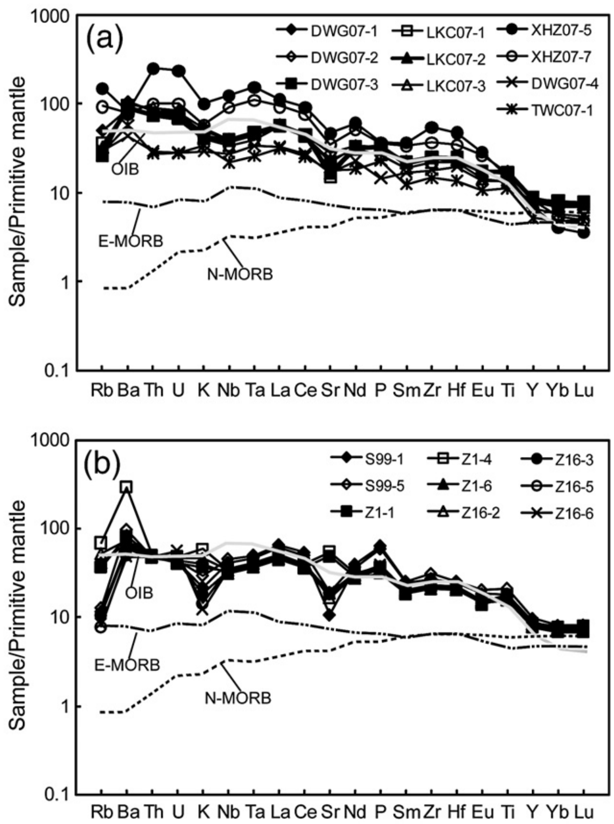

Fig. 8. Primitive mantle normalized trace elements spider diagrams of Permian basaltic rocks in the Tarim basin ((a): outcrops, (b): drill cores). Normative values are from Sun and Mcdonough (1989). Also plotted are patterns of OIB, N-MORB and E-MORB also from Sun and Mcdonough (1989).

minimum $(^{87}Sr/^{86}Sr)i$ does not correspond to maximum $\varepsilon Nd(t)$, the sample which has the largest $(^{206}Pb/^{204}Pb)t$ does not have largest $(^{207}Pb/^{204}Pb)t$ and $(^{208}Pb/^{204}Pb)t$ values and vice versa.

Fig. 9 shows the information revealed by Sr–Nd isotopes. Other Permian igneous rocks (Jiang et al., 2004a,b,c) from Keping, Mazha'ertage (Xiaohaizi) and Wajilitage are also plotted in Fig. 9 for comparison. In the $\varepsilon Nd(t)-(^{87}Sr/^{86}Sr)i$ diagram (Fig. 9), rocks of this study all plot in the field of "basin and range" (Hawkesworth et al., 1995) and are very similar to the distribution of Keping basalts (Jiang et al., 2004b), with the exceptions of DWG07-4 and XHZ07-7 which have large $\varepsilon Nd(t)$ and plot in the OIB area. Curiously, of the twenty reference samples from Mazha'ertage (Jiang et al., 2004c) and Wajilitage (Jiang et al., 2004a), most of the samples plot in the field of OIB, possibly implying that Permian igneous rocks in these two areas have mantle plume signatures. This is further supported by the occurrence of mafic to ultramafic rocks, such as olivine gabbros, picrite, dunite and pyroxenite (Jiang et al., 2004a,c).

In $(^{207}Pb/^{204}Pb)t-(^{206}Pb/^{204}Pb)t$ diagram (Fig. 10a), all samples plot within the OIB field and lie between EMI and EMII although they are closer to EMI. In $(^{208}Pb/^{204}Pb)t-(^{206}Pb/^{204}Pb)t$ diagram (Fig. 10b), the case is more complex with most samples lying within OIB and even "Atlantic–Pacific MORB" field and plot between EMI and DMM fields. Reference data of Keping and Mazha'ertage basaltic rocks are taken from Zhou et al. (2009).

6. Discussion

6.1. Temporal and spatial distribution of PBRT

Most of the PBRT are covered by aeolian sands, so it is difficult to estimate their spatial distribution. Fortunately, owing to the large scale oil exploration in the Tarim basin we have sufficient information to enable us to draw a sketch map of the Permian magmatism. In the north, central and southwest Tarim, Permian igneous rocks have been intersected in most drillholes (Jia, 1997). The extension of this Permian basaltic province (after Yang et al., 2005; Chen et al., 2006) is illustrated in Fig. 1. According to studies of Yang et al. (2005) and Chen et al. (2006), it covers an area of about 200,000 km^2 which is smaller than that of the Emeishan large igneous province (Coffin and Eldholm, 1994; Chung and Jahn, 1995; Chung et al., 1998). Several geochronologic investigations have been carried out on the Permian igneous rocks in the last two decades (e.g., Chen et al., 1997a,b, 1998; Jia, 1997; Yang et al., 2006, 2007; Li, 2007). In order to have a clear idea of the age spread, the results of previous studies have been integrated with age results from this study. In the histogram shown in Fig. 11, the age span extends from about 290 Ma to 260 Ma. There is an age peak between 270 Ma and 280 Ma with another less well defined age peak at 280 Ma–290 Ma. The ages of these two peaks account for about 76% of all the data collected, suggesting that the main body of Tarim Permian igneous rocks were emplaced during the early Permian.

6.2. Petrogenesis

6.2.1. Probable mantle source

It is generally thought that basalts derive from the melting of mantle peridotite but because of the complexity of the lithospheric mantle, the identification of a mantle source for continental basalts is a formidable task. The upper mantle can be subdivided into lithospheric mantle and asthenospheric mantle, characterized by different rheology and lithology. In the context of this paper, it is important to point out that PBRT are within-plate rocks. This conclusion can be drawn from the following: firstly, the Tarim Craton is an ancient craton which has Archean to Neoproterozoic rocks and there is no evidence that the Tarim Craton was ever fragmented since the Cambrian (Jia, 1997). Secondly, continental deposits were dominant since the Permian, in contrast to the dominance of pre-Permian marine deposits, implying a within-plate environment (Jia, 1997; Chen et al., 2006). Finally, the discrimination diagrams (Fig. 12) show that most samples plot in the within-plate field. Sources of

Table 2
Sr–Nd isotope results of Permian basaltic rocks in the Tarim basin.

Sample	Rb (ppm)	Sr (ppm)	$^{87}Rb/^{86}Sr$	$^{87}Sr/^{86}Sr$	2σ	$(^{87}Sr/^{86}Sr)i$	Sm (ppm)	Nd (ppm)	$^{147}Sm/^{144}Nd$	$^{143}Nd/^{144}Nd$	2σ	εNd(t)	TDM (Ma)
DWG07-1	28.63	343.8	0.2410	0.708329	13	0.707369aay	8.94	41.14	0.1314	0.512408	13	−2.16	1373
DWG07-4	18.52	380.8	0.1407	0.705329	14	0.704769	7.28	29.17	0.1509	0.512729	12	3.42	1022
LKC07-1	22.07	321.0	0.1991	0.708053	13	0.707260	8.96	41.15	0.1316	0.512395	11	−2.40	1399
S99-5	8.33	430.4	0.0560	0.706301	10	0.706078	12.64	59.61	0.1282	0.512392	12	−2.35	1349
TWC07-1	17.89	378.9	0.1366	0.707039	10	0.706495	5.67	26.00	0.1319	0.512382	11	−2.67	1428
XHZ07-7	56.54	711.2	0.2301	0.705726	11	0.704810	13.47	64.24	0.1267	0.512749	14	4.66	704
Z1-1	22.80	1064.4	0.0620	0.708558	9	0.708311	7.70	35.76	0.1302	0.512379	14	−2.68	1405
Z1-6	25.08	397.2	0.1827	0.707633	13	0.706905	7.62	34.86	0.1321	0.512387	13	−2.58	1423
Z16-2	32.42	358.1	0.2621	0.708112	13	0.707068	83.86	384.8	0.1318	0.512376	11	−2.79	1438
Z16-6	5.84	426.0	0.0397	0.707787	11	0.707629	8.15	37.75	0.1305	0.512402	13	−2.24	1368

Decay constants of $^{87}Rb \rightarrow ^{87}Sr$ and $^{147}Sm/^{143}Nd$ are 1.42×10^{-11} (Steiger and Jager, 1977) and 6.54×10^{-12} (Lugmair and Marti, 1978) respectively.

Table 3
Pb isotope results of Permian basaltic rocks in the Tarim basin.

Sample	$^{206}Pb/^{204}Pb$	2σ (%)	$^{207}Pb/^{204}Pb$	2σ (%)	$^{208}Pb/^{204}Pb$	2σ (%)	U (ppm)	Th (ppm)	Pb (ppm)	$(^{206}Pb/^{204}Pb)t$	$(^{207}Pb/^{204}Pb)t$	$(^{208}Pb/^{204}Pb)t$
DWG07-1	18.3370	0.02	15.5533	0.017	38.7123	0.040	1.65	6.55	9.25	18.3044	15.5516	37.6144
DWG07-4	18.0327	0.02	15.4803	0.024	38.3408	0.025	0.60	2.47	4.20	18.0068	15.4789	37.4293
LKC07-1	18.1877	0.01	15.5441	0.013	38.6464	0.013	1.54	6.52	9.55	18.1582	15.5425	37.5879
S99-5	17.9553	0.03	15.5627	0.030	38.6331	0.024	0.94	4.21	5.96	17.9265	15.5612	37.5377
TWC07-1	18.0375	0.02	15.5594	0.026	38.4633	0.031	0.59	2.36	5.15	18.0167	15.5583	37.7531
XHZ07-7	18.3169	0.01	15.6076	0.012	38.7834	0.013	2.11	8.60	20.85	18.2984	15.6067	38.1437
Z1-1	18.2554	0.01	15.5559	0.015	38.6399	0.016	0.87	4.19	5.89	18.2282	15.5545	37.5373
Z1-6	18.2602	0.02	15.5613	0.020	38.6571	0.022	0.93	4.17	5.91	18.2315	15.5598	37.5632
Z16-2	18.6279	0.02	15.5910	0.018	39.1241	0.021	1.00	4.31	3.65	18.5778	15.5884	37.2922
Z16-6	18.5775	0.03	15.5920	0.030	38.8848	0.046	1.21	4.23	4.24	18.5254	15.5893	37.3377

Decay constants of $^{238}U \rightarrow {}^{206}Pb$, $^{235}U \rightarrow {}^{207}Pb$ and $^{232}Th \rightarrow {}^{208}Pb$ are 1.55×10^{-10}, 9.85×10^{-10} and 4.95×10^{-11} respectively (Steiger and Jager, 1977).

within-plate volcanism in extensional settings are still in debate. More specifically, is the source of alkaline magmas in the lithosphere, the convecting asthenosphere or both? It is generally accepted that if the isotopic composition of basalts from within-plate regions resembles those of ocean island basalts (OIB), they are derived only from the asthenospheric mantle. However, many OIB-like lavas from within-plate settings exhibit enriched incompatible element characteristics.

Lamprophyric rocks are commonly thought to be a product of the lithospheric mantle and for this reason they can be used as a probe of lithospheric mantle. For this study, the lithospheric mantle can be excluded because the Triassic lamprophyre dikes (Chai et al., 2007) in southwest margin of Tarim show strong depletion of HFSE, much lower TiO_2 contents (0.75%–0.86%) and Nb/La, Ba/Nb and Zr/Nb ratios that differ drastically from those of the studied samples. The lithospheric mantle cannot be a contaminant of the "primary" magma, for the same reason.

In the chondrite normalized rare earth element (REE) diagram (Fig. 7) and primitive mantle normalized incompatible element spider diagram (Fig. 8), all samples bear the signature of oceanic island basalts (OIB). Element ratios, such as Nb/La, Nb/Ta and Zr/Hf, strongly resemble those of OIB (JÖrg et al., 2007) also. Moreover, positive $\varepsilon Nd(t)$ values of two samples also indicate an OIB source. Therefore it is highly probable that the PBRT have mantle origin, like that of OIB.

6.2.2. Magma processes

The low MgO, Cr and Ni contents indicate that these samples were not derived from primitive magmas. Fractionation is used by many authors to interpret geochemical characteristics observed in evolved volcanic rocks, such as decrease in mafic minerals and the increment of SiO_2 saturation. Fractionation may play an important role in magma evolution of these samples, as can be seen from the Harker diagram (Fig. 6). In Fig. 6, negative correlations exist between SiO_2 and TFe ($Fe_2O_3 + FeO$), MgO, TiO_2 and CaO, which imply fractionation of mafic minerals such as olivine, pyroxene and titanmagnetite. Moreover, ultramafic rocks in Bachu (Mazha'ertage) which formed by the accumulation of mafic minerals (Zhou et al., 2009) provide strong evidence for the existence of fractionation. Plagioclase fractionation may be minor as there is no clear negative correlation between Al_2O_3 and SiO_2. This can also be seen from the chondrite normalized REE patterns which generally display no obvious Eu negative anomalies.

Relatively large initial $^{87}Sr/^{86}Sr$ values (0.7048–0.7083) and negative $\varepsilon Nd(t)$ values (-2.79 to -2.16) of most samples with high levels of some incompatible elements indicate contamination by crustal material. The average Ce/Pb and Nb/U ratios of oceanic basalts (OIB and MORB) are 25 ± 5 and 47 ± 7, respectively (Hofmann et al., 1986), significantly higher than the values for average continental crust or arc volcanic rocks (Taylor and McLennan, 1985). Therefore the Ce/Pb and Nb/U values may be used as indicators of the source rock. In Fig. 13 most samples do not plot on to the OIB and MORB fields but

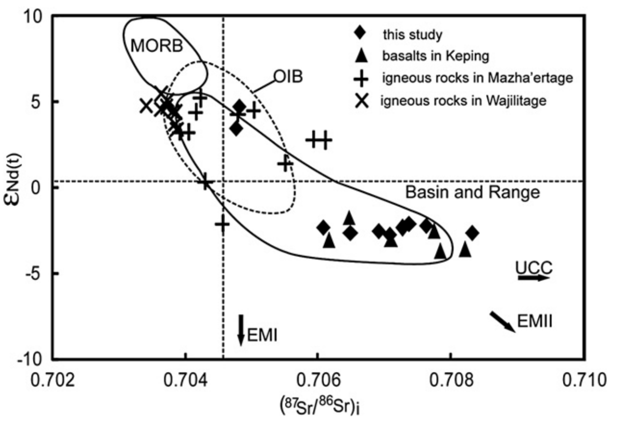

Fig. 9. $\varepsilon Nd(t) - (^{87}Sr/^{86}Sr)i$ plot (after Fan et al., 2003) of Permian basaltic rocks in the Tarim basin. Also plotted are data from Wajilitage (Jiang et al., 2004a), Keping (Jiang et al., 2004b) and Mazha'ertage (Jiang et al., 2004c).

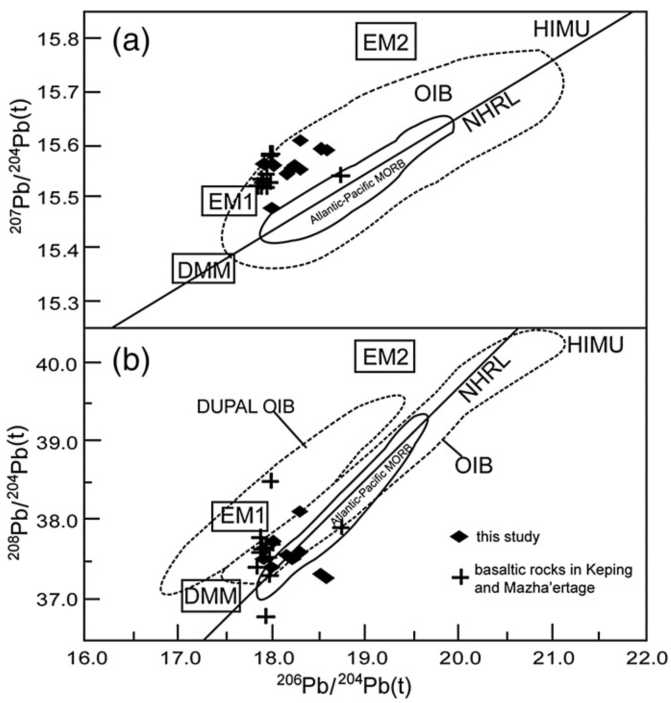

Fig. 10. Plots of $^{207}Pb/^{204}Pb(t)$ vs. $^{206}Pb/^{204}Pb(t)$ (a) and $^{208}Pb/^{204}Pb(t)$ vs. $^{206}Pb/^{204}Pb(t)$ (b) for Permian basaltic rocks in the Tarim basin. Reference values of Keping and Mazha'ertage are from Zhou et al. (2009). The field of HIMU, OIB, Dupal OIB, EM1 and EM2 are from Hawkesworth et al. (1984), Hart (1984, 1988), Hamelin and Allègre (1985), Hart et al. (1986) and Weaver (1991). The Northern Hemisphere Reference Line (NHRL) is from Hart (1984). The fields of the Indian Ocean MORB, Atlantic–Pacific MORB and Kerguelen are from Hamelin and Allègre (1985), Barling and Goldstein (1990), Deniel (1998) and references therein.

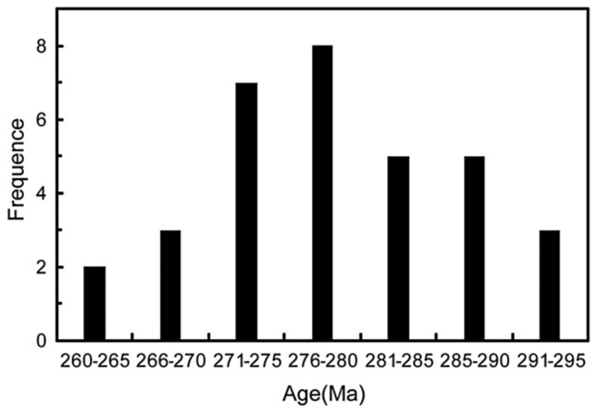

Fig. 11. Age data histogram of Permian magmatism in the Tarim basin (data comes from Chen et al., 1997a,b, 1998; Yang et al., 2006, 2007; Li, 2007 and this study).

show affinity with continental crust. In the SiO_2–$\varepsilon Nd(t)$ diagram (Fig. 14) these samples show distinct $\varepsilon Nd(t)$ values. One group has positive $\varepsilon Nd(t)$ values whilst the other has negative $\varepsilon Nd(t)$ values. It is worth noting that among the samples with negative $\varepsilon Nd(t)$ values, there seems to be no severe crustal contamination because their $\varepsilon Nd(t)$ values show small variation with increasing SiO_2 contents, also narrow range and low lead isotope ratios do not support the upper crust as a contaminant as this has much higher lead isotope ratios. It is therefore necessary to define a process or mechanism whereby the studied samples acquired their unique geochemical traits.

After segregation from a magma chamber, the melts will ascend through the lithosphere, including the lithospheric mantle and crust, to the surface. It is important to obtain information about the compositions of lithospheric mantle and crust and especially the lower crust. However, because of it being covered with a thick succession of sedimentary rocks, it is difficult to estimate the composition of the Tarim crust. According to Li et al. (2005) and Guo et al. (2005), there are Mesoproterozoic to Neoproterozoic diorites and Neoproterozoic granodiorite in central Tarim. Geochemistry (such as negative Nb–Ta and Zr–Hf anomalies) indicates that these rocks are emplaced in an island arc setting. Because the depth of these samples is at 7000 m and upper crust usually has a thickness of at least 10 km in central Tarim (Jia, 1997), they can only represent the uppermost crystalline basement of the Tarim craton. Xu et al. (2005) reported Neoprotozoic volcanic rocks from the northeast edge of Tarim, with ages that are comparable to those obtained by Guo et al. (2005), but much younger than those obtained by Li et al. (2005). Moreover, Zhang et al. (2007, 2009a) reported mafic dikes (from Quruqtage and A'kesu) and ultramafic–mafic–carbonatite and granitoids (from Qurutage) from the northern margin of Tarim. These rocks have ages of 759 Ma–820 Ma, which are similar to Neoprotozoic rocks in central Tarim and which may represent the upper crust. Interestingly, these rocks show similar island arc affinities as reported by Li et al. (2005), Guo et al. (2005) and Xu et al. (2005). Therefore, upper crust can be precluded as

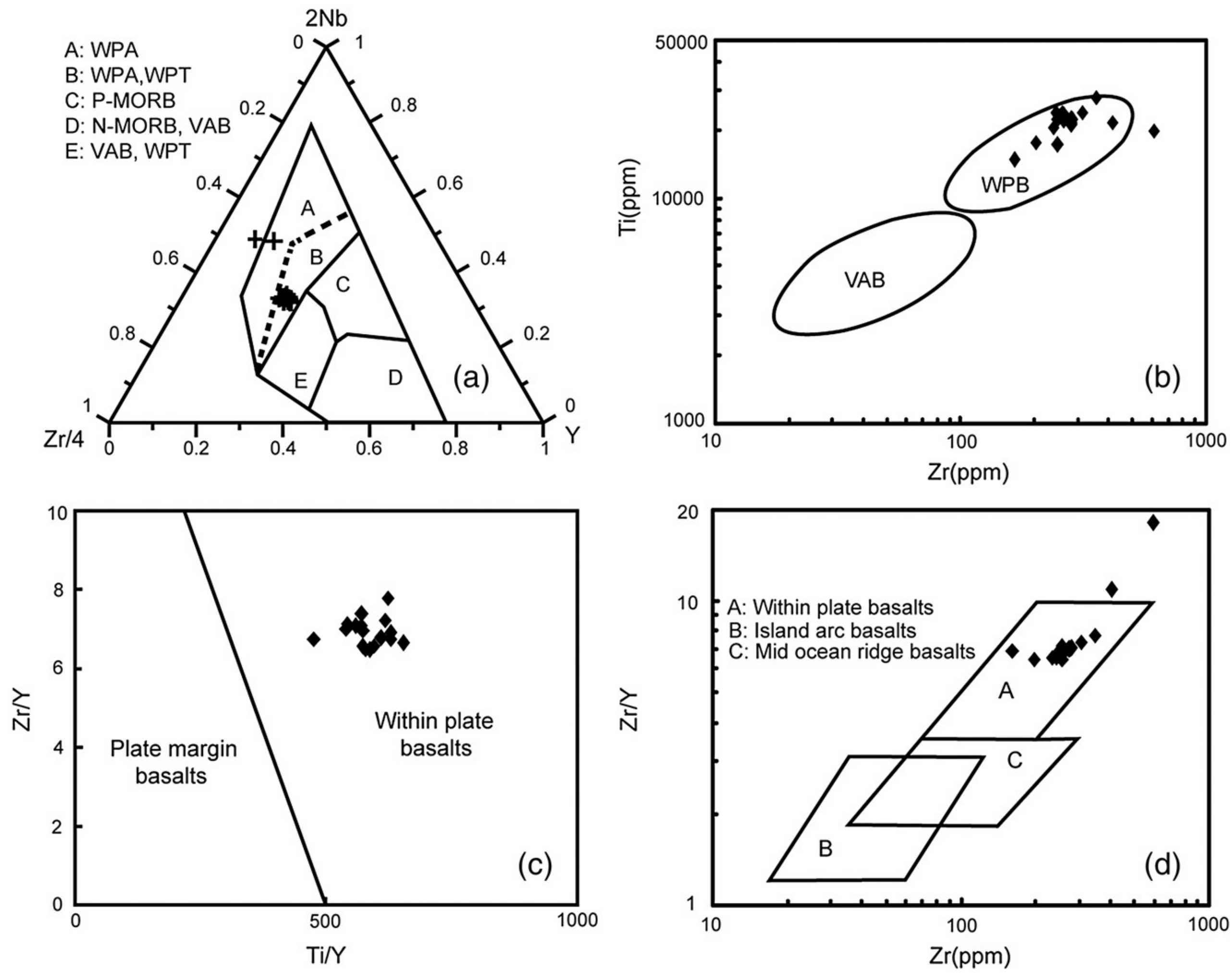

Fig. 12. Tectonic discrimination plots of Permian basaltic rocks in the Tarim basin: 2Nb-Zr/4-Y (a) (after Meschede, 1986), Ti–Zr (b) (after Pearce, 1996), Zr/Y–Ti/Y (c) (after Pearce and Gale, 1977), Zr/Y–Zr (d) (after Pearce and Norry, 1979).

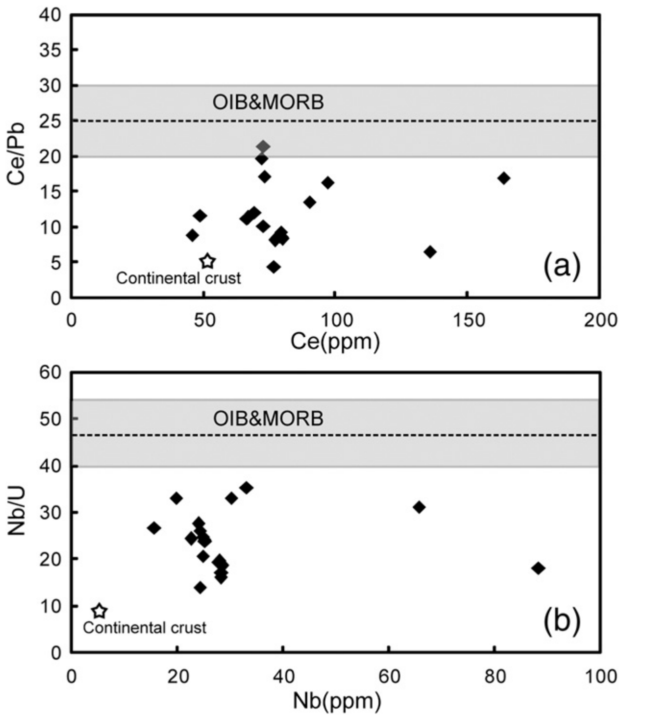

Fig. 13. Plots of Ce/Pb–Ce (a) and Nb/U–Nb (b) for Permian basaltic rocks in the Tarim basin. The extension of OIB and MORB is from Hofmann et al. (1986).

a contaminator in the generation of PBRT. The lower crust is even more elusive to characterise than the upper crust in Tarim because no granulite enclaves have been reported in central Tarim. The v_p of lower crust materials in Bachu is 6.54–6.95 km/s (Jia, 1997), which is comparable to that of granulites with different compositions. Zheng et al. (2005, 2006) reported granulite xenoliths of lower crust in Cenozoic basalts, discovered from the Tuoyun basin to the southwest of Tianshan. Because Tianshan is adjacent to the Tarim basin, the study of Tuoyun lower crust granulite contributes to a better understanding of the lower crust of Tarim. These studies revealed that the granulites formed by metamorphism of lower crustal igneous rocks. Furthermore zircon Hf isotope values (Zheng et al., 2006) indicate crustal contamination. Wu et al. (2006) reported Proterozoic OIB-like rocks in Bachu which have high REE contents and elements ratios such as Nb/La, Ba/Nb and Zr/Nb, very different from the studied samples. Investigations by Chen et al. (2006) and Wu et al. (2006) showed that Bachu district uplifts more than other places in the Tarim basin, so these OIB-like rocks probably represent lower crust in Tarim.

As discussed above, the "primitive" magma did not derive from the lithospheric mantle, nor was the "primitive" magma contaminated by lithospheric mantle or upper crust. Thus, the most probable case is

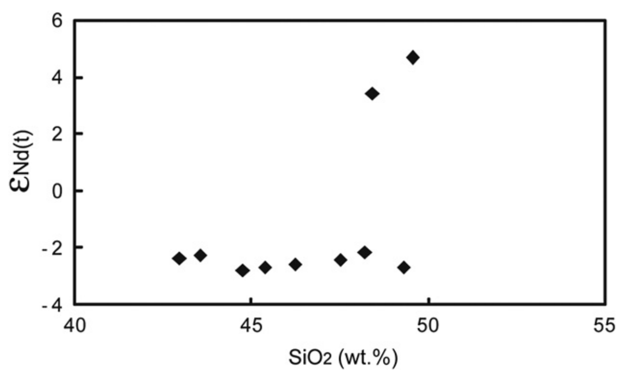

Fig. 14. The εNd(t)–SiO_2 diagram of Permian basaltic rocks in the Tarim basin.

that the "primitive" magma passed rapidly through the lithospheric mantle and came to the base of crust, where different degrees of assimilation of pre-existing OIB materials and fractionation occurred. By this mechanism the OIB patterns of REE and incompatible elements and different isotope ratios can be explained by different degrees of assimilation.

6.3. Relationship with large igneous province

The term "Large Igneous Province" (LIP) was initially proposed by Coffin and Eldholm (1991, 1992, 1993a,b, 1994) to represent a variety of mafic igneous provinces with areal extents >0.1 Mkm^2 that represented "massive crustal emplacements of predominantly mafic (Mg- and Fe-rich) extrusive and intrusive rock, and originated via processes not related to seafloor spreading." According to a definition revised by Bryan and Ernst (2008) "Large Igneous Provinces are magmatic provinces with areal extents>0.1 Mkm^2, igneous volumes >0.1 Mkm^3 and maximum lifespans of about 50 Myrs that have intraplate tectonic settings or geochemical affinities, and are characterized by igneous pulse(s) of short duration (~1–5 Ma), during which a large proportion (>75%) of the total igneous volume has been emplaced." If we employ this definition to PBRT we find it cannot be considered as a LIP: firstly, though it covers an area of about 200,000 km^2 (Yang et al., 2005; Chen et al., 2006), to make the volume exceed 0.1 Mkm^3 the average thickness should exceed 500 m, which is not the case as revealed by drilling (thickness rarely exceeds 500 m except around Keping, where there is a thickness of about 700 m). Secondly, we do not know whether more than 75% of the volume were emplaced over a short duration (~1–5 Ma), the volume of the PBRT may have been larger when it formed during Permian. More detailed work is needed before we can confirm that the PBRT is in fact a LIP.

6.4. Implication for plume–lithosphere interaction

Mantle plumes are regarded as focused upwellings that originate from deep mantle sources (Campbell et al., 1989; Campbell and Griffiths, 1990; Olson, 1990). Since the mantle plume hypothesis can explain many phenomena observed in within-plate magmatism, such as oceanic island basalts (OIB) and continental flood basalts (CFB), authors have increasingly depended on this hypothesis, although it is debatable whether or not mantle plume exists at all. Many other theories have been proposed as to the mechanisms for the derivation of large igneous provinces (Sheth, 1999; Anderson, 2000). We suggest, however, that the mantle plume theory is more appropriate for the PBRT based on the evidence listed below.

The most cogent evidence comes from Wajilitage, where Permian picritic rock cements in breccias pipes were found, indicating an anomalously high temperature (Jiang et al., 2004a) comparable to that of the mantle plume head. Picrites can also form in island arcs (Woodland et al., 2002), but as mentioned above, the Tarim was in a within-plate environment during the Permian. Moreover, according to a study by Jiang et al. (2004a), olivine phanerocrysts in picrites have forsterite (Fo) contents as high as 91%, which resemble that of Emeishan picrites (Zhang and Wang, 2004; Zhang et al., 2006), which are believed to have a mantle plume source (Xu et al., 2001; He et al., 2003). Therefore, we suggest that basalts in Tarim probably share the same origin as suggested by Dobretsov et al. (2008) for the Siberian trap. As shown by our geochemical data, however, a mantle plume may have mainly provided heat with only a minor part of the plume being melted.

Other evidence supporting the existence of a Permian mantle plume in the Tarim include: 1) high surface heat flow during the Permian. The present heat flow remains high in central Tarim (Jia, 1997), where Permian igneous rocks are most abundant. 2) Drilling records in central Tarim (Jia, 1997) show that there is an uplift in Tarim during the Permian (strata older than those of the Permian were obviously deformed, with uniform thickness precluding periods prior to Permian as the probable period during which the uplift formed). This uplift was probably caused by the impingement of the mantle plume to the lithosphere.

As previously mentioned, plume–lithosphere interaction may be an appropriate mechanism for the generation of PBRT. However, the possible consequences of plume–lithosphere interactions and even the existence of mantle plumes are widely debated (e.g., Farnetani et al., 1996; Sleep, 1997; Anderson, 1998; Ebinger and Sleep, 1998; Kukkonen and Peltonen, 1999; Sheth, 1999; Tackley, 2000; Sleep et al., 2002; Nyblade and Sleep, 2003; Sleep, 2003a,b, 2005; Ingle and Coffin, 2004; King, 2005). Thus, before we discuss plume–lithosphere interaction, attention should be paid to the thick lithosphere in the Tarim craton. Qiu et al. (2006) proposed that the lithosphere in the Tarim craton has thicknesses of about 200 km–250 km, with an average of 170 km. According to Manea et al. (2009), a thick lithosphere may act as a lid, hindering the melting of rising plume material. On this basis, we consider that a Permian mantle plume caused the uplift of the Tarim lithosphere and provided heat. At Bachu where Permian igneous activity is most obvious, there is an apparent denudation of Permian strata (Chen et al., 2006) indicating that the combination of decompression and heat facilitated the melting of the asthenospheric mantle.

We investigated the possibility of probable contaminants of asthenospheric melts. Due to their geochemical resemblance with island arc rocks, the Proterozoic crystalline upper crust (Guo et al., 2005; Li et al., 2005; Xu et al., 2005) is excluded as a possible contaminant. Lamprophyre dikes (Chai et al., 2007) in the southwest margin of the Tarim craton were formed by the enriched subcontinental lithospheric mantle (SCLM) and excluded for the same reason. The most probable contaminant is the lower crust, which has compositions similar to OIB and the following mechanism is put forward for group 2 rocks (group 1 had little assimilation during step 2): Permian mantle plume caused the uplift of the Tarim lithosphere (step 1); enriched asthenospheric mantle partially melted and the magma ascended rapidly to the base of crust where different degrees of assimilation and fractionation took place (step 2). Finally the evolved magmas erupted to the surface with little contamination of upper crust materials (step 3) (Table 4).

6.5. Tectonic significance

The Permian time is important for mantle plume activities in Euro-Asia continent, as shown by the Siberia trap and Emeishan LIP, which are thought by many researchers to be manifestations of mantle plumes (Richards et al., 1989; Campbell and Griffiths, 1990; Xu et al., 2001; He et al., 2003). One problem arises here as to why these plumes are clustered in the Permian? The analysis of the Paleozoic tectonic environments of the Tarim craton may shed some light on this enigma. To the north of Tarim, there was large scale subduction of the south Tianshan ocean basin beneath the Tarim craton during the Permian (Wang et al., 2004) or Carboniferous (Gao et al., 1998). To the south, the palaeo Tethys ocean subducted beneath the Tarim craton during the early to middle Permian (Yang et al., 2005). These subduction events have two effects in the generation of PBRT: first, the subduction made the source enriched in LREE and LILE; secondly, the subducted oceanic lithosphere may have reached the 670 km discontinuity in the mantle and may further penetrate the boundary to the core–mantle layer, thus causing a large upwelling mantle plume. In fact, the Siberian and Emeishan LIPs and the Tarim were all probably caused by mantle plumes associated with the formation of Pangea (Santosh et al., 2009). In this context, it is interesting to note that Ivanov et al. (2008) advocated that the Siberian LIP was formed by shallow mantle upwelling related to a stagnant subducted slab.

Table 4
Different evolution patterns of group 1 and group 2.

Step / Group	1	2	3	Explanations
1	Uplift of the Tarim lithosphere	Little assimilation, with fractionation	Erupted to the surface	Group 1 includes DWG07-4, XHZ07-5 and XHZ07-7. Group 2 includes the other 16 samples. The detailed meanings of steps 1, 2 and 3 can be found in the text.
2	Uplift of the Tarim lithosphere	Different degrees of assimilation and fractionation	Erupted to the surface	

7. Conclusions

From geochronological, petrological and geochemical studies of PBRT, we make the following conclusions.

1) The age span of Permian igneous activity in the Tarim spans about 30 Myrs, from 290 Ma to 260 Ma, with a peak between 270 Ma and 280 Ma and another less distinct age peak of 280 Ma–290 Ma. These two peaks account for about 76% of all the data collected.
2) Geochemically, the Permian igneous rocks of Tarim can be subdivided into two groups. Group one (DWG07-4, XHZ07-5 and XHZ07-7) is more “primitive” from the point of isotope ratios and group two (the other 16 samples) is more “evolved”. All samples show OIB-like nature in chondrite normalized REE patterns and primitive mantle normalized incompatible element patterns. Group one was generated by the melting of OIB-like asthenosphere and later fractionation with little contamination of crustal materials. Group two was generated by a mixture of asthenosphere-derived melts with preexisting OIB-like rocks and fractionation at the lower crust.
3) More evidence is needed to define unambiguously PBRT as a LIP. The PBRT was caused by plume–lithosphere interaction in which the mantle plume mainly caused lithosphere uplift and provided heat.
4) The Permian large igneous provinces such as Siberian traps, Emeishan and the PBRT were probably all generated by mantle plumes associated with subduction systems and the formation of a new supercontinent (Pangea) during the Permian.

Acknowledgements

This study was financially supported by China Petroleum & Chemical Corporation (SINOPEC) (No: YPH08064), Major State Basic Research Development Program of China (973) (No: 2009CB219301) and National Science Found Committee (No: 40803012). Doctors Q.Q. Meng, D.Y. Zhu and Q.L. Xie are thanked for their assistance in field work. We are grateful for constructive reviews by Franco Pirajno and an anonymous reviewer. Thanks are due to Valerie A. Hall for polishing the English of this article.

Appendix A. Supplementary data

Supplementary data associated with this article can be found, in the online version, at doi:10.1016/j.gr.2010.03.006.

References

Anderson, D.L., 1998. The scales of mantle convection. Tectonophysics 284, 1–17.
Anderson, D.L., 2000. The thermal state of the uppermantle; no role for mantle plumes. Geophysical Research Letters 27, 3623–3626.
Barling, J., Goldstein, S.L., 1990. Extreme isotopic variations in Heard Island lavas and the nature of mantle reservoirs. Nature 348, 59–62.
Boynton, W.V., 1984. Geochemistry of the rare earth elements: meteorite studies. In: Henderson, P. (Ed.), Rare Earth Element Geochemistry. Elsevier, pp. 63–114.
Bryan, S.E., Ernst, R.E., 2008. Revised definition of Large Igneous Provinces (LIPs). Earth-Science Reviews 86, 175–202.
Campbell, I.H., Griffiths, R.W., 1990. Implications of mantle plume structure for the evolution of flood basalts. Earth and Planetary Science Letters 99, 79–93.

Campbell, I.H., Griffiths, R.W., Hill, R.I., 1989. Melting in an Archean mantle plume: heads it's basalts, tails it's komatiites. Nature 339, 697–699.

Chai, F.M., Parat, A., Zhang, Z.C., Mao, J.W., Dong, L.H., Muhtar, Z., 2007. Geochemistry of the Lamprophyre dykes in the SW margin of the Tarim block and their source region. Geological Review 53 (1), 11–21 (in Chinese with English abstract).

Chai, F.M., Mao, J.W., Dong, L.H., Yang, F.Q., Liu, F., Geng, X.X., Zhang, Z.X., 2009. Geochronology of metarhyolite from the Kangbutiebao Formation in the Kelang basin, Altay Mountain, Xinjiang: implications for the tectonic evolution and metallogeny. Gondwana Research 16, 189–200.

Charvet, J., Shu, L., Laurent-Charvet, S., 2007. Paleozoic structural and geodynamic evolution of eastern Tianshan (NW China): welding of the Tarim and Junggar plates. Episodes 30, 162–185.

Chen, H.L., Yang, S.F., Dong, C.W., Zhu, G.Q., Jia, C.Z., Wang, Z.G., 1997a. Research on geological thermal events of Tarim basin. Chinese Science Bulletin 42 (10), 1096–1099 (in Chinese).

Chen, H.L., Yang, S.F., Dong, C.W., Jia, C.Z., Wei, G.Q., Wang, Z.G., 1997b. Confirmation of Permian basite zone in Tarim basin and its tectonic significance. Geochimica 26 (6), 77–87 (in Chinese with English abstract).

Chen, H.L., Yang, S.F., Dong, C.W., 1998. Confirmation of Permian intermediate-acid igneous rock zone and a new understanding of tectonic evolution in the northern part of the Tarim basin. Acta Mineralogical Sinica 18 (3), 370–376 (in Chinese with English abstract).

Chen, H.L., Yang, S.F., Wang, Q.H., Luo, J.C., Jia, C.Z., Wei, G.Q., Li, Z.L., He, G.Y., Hu, A.P., 2006. Sedimentary response to the Early-Mid Permian basaltic magmatism in the Tarim plate. Geology in China 33 (3), 545–552 (in Chinese with English abstract).

Chung, S.L., Jahn, B.M., 1995. Plume–lithosphere interaction in generation of the Emeishan flood basalts at the Permian–Triassic boundary. Geology 23, 889–892.

Chung, S.L., Jahn, B.M., Wu, G.Y., Lo, C.H., Cong, B.L., 1998. The Emeishan flood basalt in SW China: a mantle plume initiation model and its connection with continental break-up and mass extinction at the Permian–Triassic boundary. In: Flower, M.F.J., Chung, S.L., Lo, C.H., Lee, T.Y. (Eds.), Mantle Dynamics and Plate Interaction in East Asia. : AGU Geodynamic Series, vol. 27. AGU, Washington, D.C, pp. 47–58.

Coffin, M.F., Eldholm, O., 1991. Large Igneous Provinces: JOI/USSAC workshop report. The University of Texas at Austin Institute for Geophysics Technical Report, p. 114.

Coffin, M.F., Eldholm, O., 1992. Volcanism and continental break-up: a global compilation of large igneous provinces. In: Storey, B.C., Alabaster, T., Pankhurst, R.J. (Eds.), Magmatism and the Causes of Continental Break-up: Geological Society of London Special Publication, 68, pp. 17–30.

Coffin, M.F., Eldholm, O., 1993a. Scratching the surface: estimating dimensions of large igneous provinces. Geology 21, 515–518.

Coffin, M.F., Eldholm, O., 1993b. Large igneous provinces. Scientific American 269, 42–49.

Coffin, M.F., Eldholm, O., 1994. Large igneous provinces: crustal structure, dimensions, and external consequences. Reviews of Geophysics 32, 1–36.

Condie, K.C., 1985. Secular variation in the composition of basalts, an index to mantle evolution. Journal of Petrology 26, 545–563.

Condie, K.C., 1989. Geochemical change in basalts and andesites across the Archaean–Proterozoic boundary: identification and significance. Lithos 23, 1–18.

Deniel, C., 1998. Geochemical and isotopic (Sr, Nd, Pb) evidence for plume–lithosphere interactions in the genesis of Grande Comore magmas (Indian Ocean). Chemical Geology 144, 281–303.

Dobretsov, N.L., Kirdysahkin, A.A., Kirdyashkin, A.G., Vernikovsky, V.A., Gladkov, I.N., 2008. Modelling of thermochemical plumes and implications for the origin of the Siberian traps. Lithos 100, 66–92.

Ebinger, C.J., Sleep, N.H., 1998. Cenozoic magmatism throughout East Africa resulting from impact of a single plume. Nature 395, 1788–1791.

Fan, W.M., Guo, F., Wang, Y. Jun, Lin, G., 2003. Late Mesozoic calc-alkaline volcanism of post-orogenic extension in the northern Da Hinggan Mountains, northeastern China. Journal of Volcanology and Geothermal Research 121, 115–135.

Farnetani, C.G., Richards, M.A., Ghiorso, M.S., 1996. Petrological models of magma evolution and deep crustal structure beneath hotspots and flood basalt provinces. Earth and Planetary Science Letters 143, 81–94.

Floyd, P.A., Winchester, J.A., 1978. Identification and discrimination of altered and metamorphosed volcanic rocks using immobile elements. Chemical Geology 21, 291–306.

Gao, J., Li, M.S., Xiao, X.C., Tang, Y.Q., He, G.Q., 1998. Paleozoic tectonic evolution of the Tianshan Orogen, northwestern China. Tectonophysics 287, 213–231.

Gibson, S.A., Kirkpatrick, R.J., Emmerman, R., Schmincke, P.H., Pritchard, G., Okay, P.J., Horpe, R.S., Marriner, G.F., 1982. The trace element composition of the lavas and dykes from a 3 km vertical section through a lava pile of Eastern Iceland. Journal of Geophysical Research 87, 6532–6546.

Guo, Z.J., Yin, A., Robinson, A., Jia, C.Z., 2005. Geochronology and geochemistry of deep-drill-core samples from the basement of the central Tarim basin. Journal of Asian Earth Sciences 25, 45–56.

Hamelin, B., Allègre, C.J., 1985. Large scale regional units in the depleted upper mantle revealed by an isotopic study of the south-west India ridge. Nature 315, 196–198.

Han, C.M., Xiao, W.J., Zhao, G.C., Mao, J.W., Li, S.Z., Yan, Z., Mao, Q.G., 2006. Major types, characteristics and geodynamic mechanism of Late Paleozoic copper deposits in Northern Xinjiang, Northwestern China. Ore Geology Review 28, 308–328.

Hart, S.R., 1984. The Dupal anomaly: a large-scale isotopic anomaly in the southern hemisphere. Nature 309, 753–756.

Hart, S.R., 1988. Heterogeneous mantle domains: signature, genesis and mixing chronologies. Earth and Planetary Science Letters 90, 273–296.

Hart, S.R., Gerlach, D.C., White, W.M., 1986. A possible new Sr–Nd–Pb mantle array and consequences for mantle mixing. Geochimica et Cosmochimica Acta 50, 1551–1557.

Hawkesworth, C.J., Rogers, N.W., Van Calsteren, P.W.C., Menzies, M.A., 1984. Mantle enrichment processes. Nature 311 (27), 331–335.

Hawkesworth, C.J., Turner, S., Gallagher, K., Hunter, A., Bradshaw, T., Rogers, N., 1995. Calc-alkaline magmatism, lithospheric thinning and extension in the Basin and Range. Journal of Geophysical Research 100, 10271–10286.

He, B., Xu, Y.G., Chung, S.L., Xiao, L., Wang, Y.M., 2003. Sedimentary evidence for a rapid, kilometer-scale crustal doming prior to the eruption of the Emeishan flood basalts. Earth and Planetary Science Letters 213, 391–405.

Hegner, E., Walter, H.J., Satir, M., 1995. Pb–Sr–Nd isotopic compositions and trace element geochemistry of megacrysts and melilitites from the Tertiary Urach volcanic field: source composition of small volume melts under SW Germany. Contributions to Mineralogy and Petrology 122, 322–335.

Hofmann, A.W., Jochum, K.P., Seufert, M., White, W.M., 1986. Nb and Pb in oceanic basalts: new constraints on mantle evolution. Earth and Planet Science Letters 79, 33–45.

Huang, B.C., Xu, B., Zhang, C.X., Li, Y.A., Zhu, R.X., 2005. Paleomagnetism of the Baiyisi volcanic rocks (ca. 740 Ma) of Tarim, Northwest China: a continental fragment of Neoproterozoic western Australia? Precambrian Research 142, 83–92.

Ingle, S., Coffin, M.F., 2004. Impact origin for the greater Ontong Java plateau? Earth and Planetary Science Letters 218, 123–134.

Ivanov, A.V., Dermonterova, E.I., Rasskazov, S.V., Yasnygina, T.A., 2008. Low-Ti melts from the southeastern Siberian Traps Large Igneous Province: evidence for a water-rich mantle source? Journal of Earth System Science 117 (1), 1–21.

Jia, C.Z., 1997. Tectonic Characteristics and Oil–gas in the Tarim Basin. Beijing, Petroleum Industry Press, China (in Chinese).

Jia, C.Z., Wei, G.Q., 2002. Tectonics and oil forming traits of Tarim basin supplementary Chinese Science Bulletin 47, 1–8 (in Chinese).

Jiang, C.Y., Zhang, P.B., Lu, D.R., Bai, K.Y., Wang, Y.P., Tang, S.H., Wang, J.H., Yang, C., 2004a. Petrology, geochemistry and petrogenesis of the Keping basalts and their Nd. Sr and Pb isotopic compositions. Geological Review 50, 492–500 (in Chinese with English abstract).

Jiang, C.Y., Jia, C.Z., Li, L.C., Zhang, P.B., Lu, D.R., Bai, K.Y., 2004b. Source of the Fe-enriched-type high-Mg magma in Mazhartag region. Xinjiang. Acta Geologica Sinica 78, 770–780 (in Chinese with English abstract).

Jiang, C.Y., Zhang, P.B., Lu, D.R., Bai, K.Y., 2004c. Petrogenesis and magma source of the ultramafic rocks in Wajilitage region, western Tarim Plate in Xinjiang. Acta Petrologica Sinica 20 (6), 1433–1444 (in Chinese with English abstract).

JÖrg, A.P., Carsten, M., Andreas, S., Klaus, M., 2007. Nb/Ta and Zr/Hf in ocean island basalts—implications for crust–mantle differentiation and the fate of Niobium. Earth and Planetary Science Letters 254, 158–172.

King, S.D., 2005. Archean cratons and mantle dynamics. Earth and Planetary Science Letters 234, 1–14.

Kukkonen, I.T., Peltonen, P., 1999. Xenolith-controlled geotherm for the central Fennoscandian Shield: implications for lithosphere–astenosphere relations. Tectonophysics 304, 301–315.

Li, Y., 2007. The geochemical characteristics and genesis of the early Permian magmatic rocks in Tazhong-Bachu. Tarim basin, Doctoral thesis (in Chinese with English abstract).

Li, Y.J., Song, W.J., Wu, G.Y., Wang, Y.F., Li, Y.P., Zheng, D.M., 2005. The concealed Jinning granodiorite and diorite in central Tarim basin. Science in China (D series) 35 (2), 97–104 (in Chinese).

Li, Y.J., Wu, G.Y., Meng, Q.L., Shi, J., Feng, X.J., Zheng, M., 2008a. Active modes and mechanisms of the Paleozoic faulting in western Tarim. Chinese Journal of Geology 43 (4), 727–745 (in Chinese with English abstract).

Li, Z.L., Chen, H.L., Langmuir, C.H., Yu, X., Lin, X.B., Li, Y.Q., 2008b. Chronology and geochemistry of Taxinan basalts from the Tarim basin: evidence for Permian plume magmatism. Acta Pertrologica Sinica 25 (5), 959–970 (in Chinese with English abstract).

Lu, S.N., Li, H.K., Zhang, C.L., Niu, G.H., 2008. Geological and geochronological evidence of the Tarin craton and surrounding continental fragments. Precambrian Research 160, 94–107.

Lugmair, G.W., Marti, K., 1978. Lunar initial $^{143}Nd/^{144}Nd$: differential evolution of the lunar crust and mantle. Earth and Planetary Science Letters 39, 349–357.

Manea, V.C., Manea, M., Leeman, W.P., Schutt, D.L., 2009. The influence of plume head–lithosphere interaction on magmatism associated with the Yellowstone hotspot track. Journal of Volcanology and Geothermal Research 188, 68–85.

Meschede, M., 1986. A method of discriminating between different types of mid-ocean ridge basalts and continental tholeiites with the Nb–Zr–Y diagram. Chemical Geology 56, 207–218.

Nyblade, A.A., Sleep, N.H., 2003. Long lasting epeirogenic uplift from mantle plumes and the origin of the Southern African Plateau. Geochemistry Geophysics Geosystems 4 (2003GC000573).

Olson, P., 1990. Hotspots, swells and mantle plumes. In: Ryan, M.P. (Ed.), Magma Transport and Storage. Wiley, Chichester, pp. 33–51.

Pearce, J.A., 1982. Trace element characteristics of lavas from destructive plate boundaries. In: Thorpe, R.S. (Ed.), Andesites. J. Wiley and Sons, Chichester, pp. 525–547.

Pearce, J.A., 1996. A user's guide to basalt discrimination diagrams. In: Wyman, D.A. (Ed.), Trace Element Geochemistry of Volcanic Rocks: Applications for Massive Sulphide Exploration: Geological Association of Canada, Short Course Notes, vol. 12, pp. 79–113.

Pearce, J.A., Gale, G.H., 1977. Identification of ore-deposition environment from trace element geochemistry of associated igneous host rocks. Geological Society Special Publication 7, 14–24.

Pearce, J.A., Norry, M.J., 1979. Petrogenetic implications of Ti, Zr, Y and Nb variations in volcanic rocks. Contributions to Mineralogy and Petrology 69, 33–47.

Polat, A., Hofmann, A.W., Rosing, M.T., 2002. Boninite-like volcanic rocks in the 3.7–3.8 Ga Isua greenstone belt, West Greenland: geochemical evidence for intra-

oceanic subduction zone processes in the early Earth. Chemical Geology 184 (3–4), 231–254.
Qiu, R.Z., Li, T.D., Zhou, S., Deng, J.F., Xiao, Q.H., Geng, S.F., 2006. The Composition and Evolution of Lithosphere in China Continent. Geological Publishing House, Beijing, p. 60 (in Chinese).
Richards, M.A., Duncan, R.A., Courtillot, V.E., 1989. Flood basalts and hot-spot tracks: plume heads and tails. Science 246, 103–107.
Rogers, J.J.W., Santosh, M., 2003. Supercontinents in Earth Hostory. Gondwana Research 6, 357–368.
Santosh, M., Maruyama, S., Yamamoto, S., 2009. The making and breaking of supercontinents: some speculations based on superplumes, super downwelling and the role of tectosphere. Gondwana Research 15, 324–341.
Sengör, A.M.C., Natal'in, B.A., Burtman, U.S., 1993. Evolution of the Altaid tectonic collage and Paleozoic crustal growth in Eurasia. Nature 364, 209–304.
Shen, P., Shen, Y.C., Liu, T.B., Meng, L., Dai, H.W., Yang, Y.H., 2009. Geochemical signature of porphyries in the Baogutu porphyry copper belt, western Junggar, NW China. Gondwana Research 16, 227–242.
Sheth, H.C., 1999. Flood basalts and large igneous provinces from deep mantle plumes: fact, fiction, and fallacy. Tectonophysics 311, 1–29.
Sleep, N., 1997. Lateral flow and ponding of starting plume material. Journal of Geophysical Research 102, 10001–10012.
Sleep, N., 2003a. Survival of Archean cratonal lithosphere. Journal of Geophysical Research 108, 2302.
Sleep, N.H., 2003b. Geodynamic implications of xenolith geotherms. Geochemistry Geophysics Geosystems 4 (2003GC000511).
Sleep, N.H., 2005. Evolution of continental lithosphere. Annual Reviews Earth and Planetary Science 33, 369–393.
Sleep, N.H., Ebinger, C.J., Kendall, J.-M., 2002. Defection of mantle plume material by cratonic keels. In: Fowler, C.M.R., Ebinger, C.J., Hawkesworth, C.J. (Eds.), The Early Earth: Physical, Chemical and Biological Development: Geological Society London, Special Publication, vol. 199, pp. 135–150.
Song, W.J., Li, Y.J., Hu, S.L., Guo, H., Huang, Z.B., Zheng, D.M., 2003. Restudy on the $^{40}Ar/^{39}Ar$ age of Wajilitage basic–ultrabasic complex in western basin. Xinjiang Petroleum Geology 24 (4), 284–285 (in Chinese with English abstract).
Steiger, R.H., Jager, E., 1977. Subcommision on geochronology: convention of the use of decay constants in geo- and cosmochronology. Earth and Planetary Science Letters 36, 359–362.
Sun, S.S., McDonough, W.F., 1989. Chemical and isotopic systematics of oceanic basalts: implications for mantle composition and processes. In: Saunders, A.D., Norry, M.J. (Eds.), Magmatism in the Ocean Basins: Geological Society Special Publication, 42, pp. 313–345.
Tackley, P.J., 2000. Mantle convection and plate tectonics; toward an integrated physical and chemical theory. Science 288, 2002–2007.
Taylor, J.R., 1982. An Introduction to Error Analysis: The Study of Uncertainties in Physical Measurements. University Science Books, Mill Valley, Calif, p. 270.
Taylor, S.R., McLennan, S.M., 1985. The Continental Crust: Its Composition and Evolution. Blackwell Scientific Publication, pp. 209–230.
Wang, G.L., Peng, G.X., Qiu, B., Lei, G.L., Nie, C.J., Luo, J.C., Huang, Z.B., 2004. A preliminary study on lower Permian sandstone from the Kezibulake profile in NW margin of Tarim basin. Chinese Journal of Geology 39 (4), 599–603 (in Chinese with English abstract).
Xie, X., Yan, M., Li, L., Shen, H., 1989. Usable values for Chinese standard reference samples of stream sediments, soils, and rocks: GSD 9-12, GSS 1-8 and GSR 1-6. Geostandards. Newsletter 9, 277–280.
Wang, F., Zhou, X.H., Zhang, L.C., Ying, J.F., Zhang, Y.T., Wu, F.Y., Zhu, R.X., 2006a. Late Mesozoic volcanism in the Great Xing'an range (NE China): timing and implications for the dynamic setting of NE Asia. Earth and Planetary Science Letters 251, 179–198.
Wang, H.Z., He, G.Q., Zhang, S.H., 2006b. The geology of China and Mongolia. Earth Science Frontiers 13 (6), 1–13 (in Chinese with English abstract).
Weaver, B.L., 1991. The origin of ocean island basalt end-member compositions: trace element and isotopic constraints. Earth and Planetary Science Letters 104, 381–397.
Winchester, J.A., Floyd, P.A., 1977. Geochemical discrimination of different magma series and their differentiation products using immobile elements. Chemical Geology 20, 325–343.
Wood, D.A., Joron, J.L., Treuil, M., 1979. A re-appraisal of the use of trace elements to classify and discriminate between magma series erupted in different tectonic settings. Earth and Planetary Science Letters 45, 326–336.
Woodland, S.J., Pearson, D.G., Thirlwall, M.F., 2002. A platinum group element and Re–Os isotope investigation of siderophile element re-cycling in subduction zones: comparison of Grenada, Lesser Antilles arc, and the Izu-Bonin arc. Journal of Petrology 43, 171–198.
Wu, G.Y., Li, Y.J., Wang, G.L., Zheng, W., Luo, J.C., Meng, Q.L., 2006. Jinning ocean island volcanic rocks in Bachu, west Xinjiang. Geoscience 20 (3), 361–369 (in Chinese).
Xiao, W.J., Kusky, T., 2009. Geodynamic processes and metallogenesis of the Central Asian and related orogenic belts. Gondwana Research 16, 167–169.
Xiao, W.J., Zhang, L.C., Qin, K.Z., Sun, S., Li, J.L., 2004. Paleozoic accretionary and collisional tectonics of the Eastern Tianshan (China): implications for the continental growth of central Asia. American Journal of Science 304, 370–395.
Xiao, W.J., Huang, B.C., Han, C.M., Sun, S., Li, J.L., 2010. A review of the western part of the Altaids: a key to understanding the architecture of accretionary orogens. Gondwana Research 18, 253–273.
Xinjiang Bureau of Geology and Mineral Resources (XJBGMR), 1993. Regional Geology of the Xinjiang Uygur Autonomous Region. Geological Publishing House, Beijing (in Chinese).
Xu, Y.G., Chung, S.L., Jahn, B.M., Wu, G.Y., 2001. Petrologic and geochemical constraints on the petrogenesis of Permian–Triassic Emeishan flood basalts in southwestern China. Lithos 58, 145–168.
Xu, B., Jian, P., Zhang, H.F., Zou, H.B., Zhang, L.F., Liu, D.Y., 2005. U–Pb zircon geochronology and geochemistry of Neoproterozoic volcanic rocks in the Tarim block of northwest China: implications for the breakup of Rodinia supercontinent and Neoproterozoic glaciations. Precambrian Research 136, 107–123.
Yang, S.F., Chen, H.L., Dong, C.W., Jia, C.Z., Wang, Z.G., 1996. The discovery of Permian syenite inside Tarim basin and its geodynamic significance. Geochemica 25, 121–128 (in Chinese with English abstract).
Yang, S.F., Chen, H.L., Ji, D.W., Li, Z.L., Dong, C.W., Jia, C.Z., Wei, G.Q., 2005. Geological process of early Permian magmatism in Tarim basin and its geodynamic significance. Geological Journal of China University 11 (4), 504–511 (in Chinese with English abstract).
Yang, S.F., Li, Z.L., Chen, H.L., Xiao, W.J., Y X, Lin, X.B., Shi, X.G., 2006. Discovery of a Permian quartz syenitic porphyritic dyke from the Tarim Basin and its tectonic implications. Acta Petrologica Sinica 22, 1405–1412 (in Chinese with English abstract).
Yang, S.F., Li, Z.L., Chen, H.L., Santosh, M., Dong, C.W., Yu, X., 2007. Permian bimodal dyke of Tarim Basin, NW China: geochemical characteristics and tectonic implications. Gondwana Research 12, 113–120.
York, D., 1969. Least squares fitting of a straight line with correlated errors. Earth and Planetary Science Letters 5, 320–324.
Zhang, Z.C., Wang, F.S., 2002. Geochemistry of the two types of basalts of the Emeishan Basaltic Province: evidences for mantle plume–lithosphere interaction. Acta Geologica Sinica 76 (2), 138–147.
Zhang, Z.C., Wang, F.S., 2004. Implications of Mg-rich olivine and Cr-rich spinel in picrites of E'meishan continental flood basalt provinces. Progress in Natural Sciences 14 (1), 70–74 (in Chinese).
Zhang, C.L., Wang, Z., Shen, J.L., Bi, H., Guo, K.Y., Wang, A.G., 2003a. Zircon SHRIMP dating and geochemistry characteristics of Akazi rock mass of western Kunlun. Acta Petrologica Sinica 19, 523–529 (in Chinese with English abstract).
Zhang, C.L., Yang, C., Shen, J.L., Wang, A.G., Zhao, Y., Dong, Y.G., Guo, K.Y., 2003b. Zircon SHRIMP age of Neoproterozoic gneissoid in the west Kunlun and its significance. Geological Review 15 (3), 239–244 (in Chinese with English abstract).
Zhang, Z.C., Mahoney, J.J., Mao, J.W., Wang, F.S., 2006. Geochemistry of picritic and associated basalt flows of the western Emeishan flood basalt province, China. Journal of Petrology 47 (10), 1997–2019.
Zhang, C.L., Li, X.H., Li, Z.X., Lu, S.N., Ye, H.M., Li, H.M., 2007. Neoproterozoic ultramafic–mafic–carbonatite complex and granitoids in Quruqtagh of northeastern Tarim block, western China: geochronology, geochemistry and tectonic implications. Precambrian Research 15, 149–169.
Zhang, C.L., Li, Z.X., Li, X.H., Ye, H.M., 2009a. Neoproterozoic mafic dyke swarms at the northern margin of the Tarim block, NW China: age, geochemistry, petrogenesis and tectonic implications. Journal of Asian earth Sciences 35, 167–179.
Zhang, Z.C., Zhou, G., Kusky, T.M., Yan, S.H., Chen, B.L., Zhao, L., 2009b. Late Paleozoic volcanic record of the Eastern Junggar terrane, Xinjiang, Northwestern China: major and trace element characteristics, Sr–Nd isotopic systematic and implications for tectonic evolution. Gondwana Research 16, 201–215.
Zhang, Z.Y., Zhu, W.B., Shu, L.S., Wan, J.L., Yang, W., Su, J.B., Zheng, B.H., 2009c. Apatite fission track thermochronology of the Precambrian Aksu blueschist, NW China: implications for thermo-tectonic evolution of the north Tarim basement. Gondwana Research 16, 182–188.
Zhao, G.C., He, Y.H., Sun, M., 2009a. The Xiong'er volcanic belt at the southern margin of the North China Craton: petrographic and geochemical evidence for its outboard position in the Paleo-Mesoproterozoic Columbia Supercontinent. Gondwana Research 16, 170–181.
Zhao, Z.H., Xiong, X.L., Wang, Q., Bai, Z.H., Qiao, Y.L., 2009b. Late Paleozoic underplating in North Xinjiang: evidence from shoshonites and adakites. Gondwana Research 16, 216–226.
Zheng, J.P., Luo, Z.H., Yu, C.M., Yu, X.L., Zhang, R.S., Lu, F.X., Li, H.M., 2005. Zircon chronology and geochemistry of granulite xenoliths in Tuoyun, Xinjiang: petrogenesis and lower crust character in SW Tianshan. Chinese Science Bulletin 50 (8), 793–801 (in Chinese).
Zheng, J.P., Griffin, W.L., O'Reilly, S.Y., Zhang, M., Pearson, N., 2006. Granulite xenoliths and their zircons, Tuoyun, NW China: insight into southwestern Tianshan lower crust. Precambrian Research 145, 159–181.
Zhou, M.F., Zhao, J.H., Jiang, C.Y., Gao, J.F., Wang, W., Yang, S.H., 2009. OIB-like, heterogeneous mantle sources of Permian basaltic magmatism in the western Tarim Basin, NW China: implications for a possible Permian Large Igneous Province. Lithos 113, 583–594.
Zhu, D.Y., Jin, Z.J., Hu, W.X., Zhang, X.F., 2008. Effects of deep fluid on carbonates reservoir in Tarim Basin. Geological Review 54 (3), 348–357 (in Chinese with English abstract).